Redox Biology 67 (2023) 102864

Contents lists available at ScienceDirect

Redox Biology

journal homepage: www.elsevier.com/locate/redox

Natural mutations of human *XDH* promote the nitrite (NO_2^-)-reductase capacity of xanthine oxidoreductase: A novel mechanism to promote redox health?

G. Massimo [a,1], R.S. Khambata [a,1], T. Chapman [b], K. Birchall [b], C. Raimondi [a], A. Shabbir [a], Nicki Dyson [a], K.S. Rathod [a], C. Borghi [c], A. Ahluwalia [c,*]

[a] *William Harvey Research Institute, Barts & the London Faculty of Medicine & Dentistry, Queen Mary University of London, Charterhouse Square, London, EC1M 6BQ, UK*

[b] *LifeArc, Accelerator Building Open Innovation Campus, Stevenage, SG1 2FX, UK*

[c] *Department of Medical and Surgical Sciences, Faculty of Medicine, University of Bologna, Via Massarenti, N.9, 40138, Italy*

ARTICLE INFO

Keywords:
Xanthine oxidoreductase
Non-synonymous mutations
Superoxide anion
Nitrite-reductase activity
Uric acid
Nitrate-nitrite-nitric oxide

ABSTRACT

Several rare genetic variations of human *XDH* have been shown to alter xanthine oxidoreductase (XOR) activity leading to impaired purine catabolism. However, XOR is a multi-functional enzyme that depending upon the environmental conditions also expresses oxidase activity leading to both O_2^- and H_2O_2 and nitrite (NO_2^-) reductase activity leading to nitric oxide (·NO). Since these products express important, and often diametrically opposite, biological activity, consideration of the impact of XOR mutations in the context of each aspect of the biochemical activity of the enzyme is needed to determine the potential full impact of these variants. Herein, we show that known naturally occurring *hXDH* mutations do not have a uniform impact upon the biochemical activity of the enzyme in terms of uric acid (UA), reactive oxygen species (ROS) and nitric oxide ·NO formation. We show that the His1221Arg mutant, in the presence of xanthine, increases UA, O_2^- and NO generation compared to the WT, whilst the Ile703Val increases UA and ·NO formation, but not O_2^-. We speculate that this change in the balance of activity of the enzyme is likely to endow those carrying these mutations with a harmful or protective influence over health that may explain the current equipoise underlying the perceived importance of *XDH* mutations. We also show that, in presence of inorganic NO_2^-, XOR-driven O_2^- production is substantially reduced. We suggest that targeting enzyme activity to enhance the NO_2^--reductase profile in those carrying such mutations may provide novel therapeutic options, particularly in cardiovascular disease.

1. Introduction

The pathophysiological role of xanthine oxidoreductase (XOR) (EC 1.17.3.2), despite being discovered in 1902, remains uncertain. The gene (*XDH*) encoding for human XOR is transcribed as xanthine dehydrogenase (XDH), which is thought to be the main biochemical isoform expressed in humans under physiological conditions. However, under pathological conditions such as ischemia-reperfusion, inflammation and hypertension XDH can be reversibly or irreversibly converted to the oxidase form of the enzyme (XO) via oxidation of cysteine residues (Cys535, Cys992) or proteolytic cleavage of lysine (Lys 551, Lys 569) respectively [1,2]. XOR belongs to the molybdenum-containing enzyme family and exists as a homodimer of ~300 kDa with each monomer composed of three main domains: an 85 kDa *C*-terminal domain containing the molybdo-pterin-binding site (Mo–Pt), an *N*-terminal domain of 20 kDa containing two non-identical iron-sulphur (Fe–S) clusters, and an intermediate domain of 40 kDa which is the flavin adenine dinucleotide (FAD) domain.

Both XDH and XO, at the Mo–Pt binding site, catalyse two consecutive hydroxylation reactions of hypoxanthine to xanthine and xanthine to uric acid (UA) [3]. However, at the FAD site, nicotinamide adenine dinucleotide (NAD^+) is the main electron acceptor for XDH and is

* Corresponding author. William Harvey Research Institute, Barts & The London Faculty of Medicine & Dentistry, Queen, Mary University of London, Charterhouse Square, London, EC1M 6BQ, UK.
E-mail address: a.ahluwalia@qmul.ac.uk (A. Ahluwalia).

[1] These authors contributed equally to this work.

https://doi.org/10.1016/j.redox.2023.102864
Received 6 August 2023; Received in revised form 24 August 2023; Accepted 25 August 2023
Available online 4 September 2023

reduced to nicotinamide adenine dinucleotide hydrogen (NADH). In contrast, O_2 is the only electron acceptor for XO at the FAD site, leading to the formation of superoxide anion ($O_2^{\cdot-}$) and hydrogen peroxide (H_2O_2) [4]. It is noteworthy that under conditions such as ischemia-reperfusion injury, where NADH levels rise, both XDH and XO operate as NADH-oxidase enzymes, to generate $O_2^{\cdot-}$ and H_2O_2 [5,6]. This activity is independent of the Mo–Pt binding site and can be blocked by diphenyleneiodonium (DPI), a non-specific inhibitor of the flavin group [5,7]. Electrons generated from NADH oxidation can also be used at the Mo–Pt domain, for the one electron reduction of inorganic nitrite (NO_2^-) to generate the beneficial molecule nitric oxide (·NO) [6,8]. Indeed, XOR has been recognized as the most prominent enzyme responsible for NO_2^- bioactivation in the disease setting [9]. We have recently defined the NO_3^--NO_2^-NO pathway as "non-canonical" to the NO synthases-driven "canonical" pathway [9].

Whilst XOR is important for healthy purine catabolism, elevation in activity of the enzyme and build-up of UA, likely through pro-oxidant effects, is pathogenic in gout [10], metabolic disorders [11], and potentially in CVD progression [12], particularly hypertension [13,14]. In addition, much evidence has suggested that XOR-derived $O_2^{\cdot-}$ is pathogenic leading to oxidative stress and endothelial dysfunction [12]. Both of these metabolites, UA and $O_2^{\cdot-}$, have been linked robustly with disease pathology. However, there is growing appreciation of a third aspect of the biochemical activity of XOR as a nitrite reductase [15]. Perhaps, more importantly unlike both UA and $O_2^{\cdot-}$, the NO generating capacity of XOR has been linked only with protective and beneficial effects [9]. Perhaps even more salient, it has been suggested that in generating NO from nitrite at the Mo–Pt-site of XOR, this is associated with the generation of protective NO but also with simultaneous reduction in pathogenic $O_2^{\cdot-}$ and UA levels [16–18].

Naturally occurring nonsynonymous mutations in h*XDH* have been identified, with the majority leading to the rare disorders of hereditary Xanthinuria Type I and II [19–21] and prevent purine metabolism causing consequent build-up of hypoxanthine and xanthine. Some published polymorphisms are thought to be relevant for CVD and are localized to intron segments of the gene [22–24], in addition to non-synonymous mutations [20,25–28]. The minor allele frequencies (MAF) of these variants (https://gnomad.broadinstitute.org; http://phase3browser.1000genomes.org/index.html) indicate a prevalence of 1–11%. Recent large-scale studies interrogating genetic associations with gout and/or relevant CVD have not highlighted mutations in *hXDH*, but rather genes associated with UA metabolism and clearance [29–32]. However, some relatively small studies have linked specific h*XDH* variants with common disease, particularly in Asians. For instance in 196 Japanese individuals, a single nucleotide polymorphism (SNP) in the promoter region of h*XDH*, when reproduced in vitro demonstrated altered XOR expression levels [33]. Another small study (185 patients, 370 controls) described specific variants linked with oxidative stress and hypertension [24] and resonates with a study in Europeans with hypertension linking UA levels and *hXDH* mutations [22]. Many of the identified variants have been tested for functional impact upon enzyme activity in vitro. Kudo et al., in 2007, found two SNPs, 3662 A > G and 2107 A > G, leading to His1221Arg and Ile703Val mutations respectively, showing nearly a two-fold higher UA synthesis when compared with WT [27]. However, how these variants impact all aspects of XOR activity particularly the NO_2^- reductase activity of the enzyme either alone or in context with its other biochemical activities is unknown [15]. To explore this, we expressed several well described h*XDH* mutations in HEK-transfected cells and assessed all three aspects of XOR activity to better ascertain any potential functional impact of these mutations.

2. Material and methods

2.1. hXDH mutation computational predicted crystal structure

Using the 2EIQ structure, which is a 2.6 Å resolution full length human structure we analysed the impact of four very well described h*XDH* mutations upon the structure of the protein. The Schrodinger protein preparation wizard was used to assign bond orders, add hydrogen atoms and optimise tautomer, rotamer and protonation states at pH 7.0, finishing with a restrained minimisation (OPLS2005 force field with convergence of heavy atoms to 0.3 Å RMSD) to relieve any crystallographic strain. The amino acid mutations were performed in Maestro (2019 version) by selecting the lowest energy rotamer, then performing a simple minimisation restricted to residues within 5 Å of the mutated residue.

2.2. *hXDH* subcloning

h*XDH* wild type (WT) cDNA (kind gift of Professor Richard M. Wright) was excised from a pcDNA3.1-myc-hisA plasmid vector using *Nhe*I-HF and *Eco*RV-HF (New England Biolab) restriction enzymes (REs). Following purification, a Kpn-I sequence at the 3' of the cDNA was introduced and then cut with *Nhe*I-HF and *Kpn*I-HF and a GFP-tagged ligation product, pEGFP-N1 – h*XDH* introduced for visualisation of expression. Sequence was verified via Sanger sequencing (Applied Biosystems 3730 capillary sequencer) and interpreted using BioEdit Sequence Alignment Editor Software before proceeding with the site directed mutagenesis.

2.3. Site directed mutagenesis

Mutagenic primers, shown in Table S1 (This article contains supporting information), were designed using NEBaseChanger software (http://nebasechanger.neb.com). Using a Q5® Site-Directed Mutagenesis Kit (New England Biolab) we reproduced 4 non-synonymous mutations (Table 1). These variants were chosen due to previous studies identifying substantial change in conventional XOR activity and include mutations that lead to direct alterations in structure to the Mo–Pt (Ile703Val, His1221Arg, Asn909Lys) and FAD (Trp336Ala/Phe337Leu) subunits of the enzyme [27,34].

PCR conditions used for each mutant isoform are shown in Table S2 (This article contains supporting information). NEB 5-alpha competent *E. coli* cells (New England Biolab) were used for bacterial transformation. Up to three resistant colonies per mutation were selected and plasmid DNA was extracted using a QIAprep Spin Miniprep Kit (Qiagen) and quantified using a nanodrop spectrophotometer (ND.1000). Mutations were confirmed via Sanger Sequencing as above using primers reported in Table S3 (This article contains supporting information). Mutated Plasmid cDNAs were then prepared and extracted using the Qiagen® Plasmid maxi Kit.

2.4. HEK-293 transfection and stable cell line formation

Human embryonic kidney cells (HEK-293) were chosen to stably express the wild-type and all mutated variants as previous findings suggest that they do not express XDH [35] an observation confirmed in The Human Protein Atlas (https://www.proteinatlas.org/ENSG00000158125-XDH/cell+line). To produce stable cell lines of WT and mutated hXDH, 3×10^5 cells per well were seeded into a 6-well plate in high-glucose Dulbecco's modified Eagle's (DMEM) medium (Merck, UK) enriched with 10% FBS (Sigma-Aldrich), 1% L-glutamine

Table 1
Summary table indicating nucleotide substitution, exon position, amino acid changes and SNP ID for each investigated h*XDH* mutant.

Variant	Position	Nucleotide change	Type	Subunit position	Exon	SNP ID	MAF	MAF ##gnomAD					
								Europe	Asian	American	African	Jewish	Other
Asn909Lys	2727	C > A	SNP	Mo-Pt	25	rs566362	< 0.01						
His1221Arg	3662	A > G	SNP	Mo-Pt	34	rs200915287	< 0.01						
Ile703Val	2107	A > G	SNP	Mo-Pt	20	rs17011368	0.05	0.0319	0.0186	0.0210	0.1156	0.0510	0.0350
Trp336Ala/Phe337Leu	1006/1007	TG > GC	AP	Cluster of XDH/XO conversion	11		< 0.01						

(Sigma-Aldrich), 1% penicillin/streptomycin, until at 60–70% confluency. The plasmid constructs were transfected using Lipofectamine® 2000 Reagent (Invitrogen) as per the manufacturer's instructions72 h after transfection 1.2 mg/ml of G-418 (Sigma-Aldrich), previously determined via a kill-curve, was added to DMEM normal medium until single colonies appearance. 4–5 colonies per mutations were then expanded and XOR expression levels checked via immunoblotting. Only colonies with the highest expression profile were expanded, amplified, and stored in liquid N_2 for future experiments.

2.5. Cell culture and cell lysate extraction

HEK-293 cells were maintained in high-glucose DMEM medium supplied with 10% FBS, 1% L-glutamine and 1% Penicillin/Streptomycin, and G-418 (Sigma-Aldrich) 0.3 mg/ml. Cells were cultured under 5% CO_2 and at 37 °C and split every 72 h at 70–80% confluency. To prepare cell lysate, cells were cultured till 80–90% confluency and cell pellets stored at −80 °C until the day of use. For protein extraction in 200 μl PBS containing 1% Triton X, with 5.7 μM benzamidine, 1.5 μM antipain, 0.15 μM aprotinin, 4.2 μM leupeptin, 1.5 μM pepstatin A and 400 μM AEBSF protease inhibitor was added to the cell pellet and the pellet mechanically disrupted using a 25G needle (0.5 mm). The resulting homogenate was centrifuged at 4°C for 10 min at 14,000 RPM and the supernatant collected. Protein concentration was determined using a Pierce® BCA Protein Assay Kit (Thermoscientific, UK) according to manufacturer guidelines.

2.6. Quantitative real-time PCR

mRNA expression was determined in HEK-293 stable cell lines using RT-PCR. The primer sequences used are shown in Table S4 (This article contains supporting information). 5×10^6 cells were processed as per the manufacturer's instruction using the NucleoSpin RNA, Mini kit for RNA purification (Macherey Nagel, MN). RNA was converted to cDNA and RT-PCR assays conducted using SYBR green ROX mix (Thermo Scientific Abgene, UK) in 384 well plates. An ABI7900 HT Realtime PCR System (Applied Biosystems®, Life Technologies, UK), with SDS 2.3 computer software, was used to run and analyse plates. Each sample was measured in triplicate and the average taken to represent n = 1. Gene expression was measured relative to β-actin and GAPDH housekeeping genes, and expressed relative to h*XDH* WT.

2.7. Immunoblotting

Cell lysates were subjected to SDS/PAGE (0.1% w/v) immunoblotting analysis using an anti-human XOR rabbit antibody (1:2000, Abcam 133,268 RRID: AB_11154903). Briefly, 50 μg of protein of each cell extract, was prepared for electrophoresis and loaded onto an 8–16% Mini-Protean TGX gels (Bio-rad). Following this, electrophoresed proteins were transferred via a semi-dry transfer method to a 0.2 μm nitrocellulose membrane (Amersham™ Proton™). Red Ponceau solution was used to confirm transfer prior to overnight incubation with primary antibody. The membrane was then washed and then incubated with an anti-rabbit secondary antibody (1:5000, InvitrogenAB_2,536,381) for 1 h. The levels of protein were expressed relative to GAPDH expression (1:5,000, ThermoFisherScientific #AM4300, RRID: AB_2536381). The nitrocellulose membrane was exposed to a 1:1 v/v solution of Clarity Western ECL Substrate (Bio-rad) for 5 min and chemiluminescence quantified and analysed using FluorChem E software (ProteinSimple).

2.8. Confocal microscopy

A 1% gelatin (Sigma-Aldrich) pre-coated 12 mm diameter coverslip (Epredia™ Menzel™, Fisher Scientific) was placed in each well of a 24-well plate and 10^5 cells added and cultured until 70–80% confluency.

Cells were then fixed with 4% paraformaldehyde for 15 min at room temperature after which wells were rinsed three times with PBS prior to addition of 500 μl permeabilization solution (PBS + 0.25% Triton X-100). After washing with PBS a 2.5% BSA solution was applied for 1 h and then incubated with primary anti-human XOR rabbit antibody (1:25, Abcam 133,268 RRID: AB_11154903) and left over-night at 4 °C. The following day coverslips were washed with PBS and incubated with the secondary antibody, Alexa Fluor™ 555 donkey anti-rabbit (1:250, Life Technologies, RRID: AB_10892947) for 1 h at room temperature. Each coverslip was then washed prior to incubation with PBS + DAPI (1:5000) staining solution. For each mutant two coverslips were analysed for each experiment with XOR expression visualized under a confocal microscope (LSM 880 with Airyrscan equipped with an Apochromat 63 × ; 1.4 numerical aperture (NA) oil objective (Zeiss, Germany)).

2.9. Flow cytometry for XOR

5×10^5 cells were fixed and permeabilised (Intracellular fixation and permeabilization buffer, Thermofisher, UK) and then incubated with 2% donkey serum followed by anti-human xanthine oxidase (1:1000; ab133268, Abcam, UK; RRID: AB_11154903), for 30min at 21 °C. Cells were then washed and the secondary antibody (donkey anti-rabbit IgG preadsorbed, Abcam, RRID: AB_2715515) incubated for 30min 21 °C. Samples were analysed using a BD LSRFortessa Flow Cytometer, and data recorded using BD FACSDiva analysis software. Histogram images were produced using FlowJo v10.7.2.

2.10. Pterin-based fluorimetric assay of XDH/XO activity

To determine the relative proportions of XDH versus XO activity for each mutant we used a modified protocol as described by Beckman et al. (1989) [36]. 1000 μg of cell lysate protein, obtained as above, was mixed with pre-warmed PBS (50 mM) + Na_2-EDTA (0.1 mM) buffer pH 7.4 in a final volume of 200 μl. Baseline fluorescence was measured every 20 s for 5 min. XO activity was measured by adding pterin (10 μM) whereas XDH + XO activity was quantified in the presence of 10 μM methylene blue. The reaction was stopped by adding 10 μM allopurinol before reading the fluorescence produced by isoxanthopterin (1 μM), used as an internal standard. Stock solutions were made fresh every day; 100 mM of pterin and 10 mM of isoxanthopterin stock solutions were prepared in NaOH 1 N, and then serially diluted in PBS buffer. 10 mM methylene blue was prepared in MilliQ H_2O and diluted as required. Fluorescence was measured using a Tecan i-control plate reader (infinite M200 Pro) excited at 345 nm and with emission at 390 nm. The fluorescence data was corrected for the immediate fluorescence increase after isoxanthopterin addition, and calculated using the following formula:

$$U = \{\Delta F \text{ x } s\text{-}^{1} \text{ x } [IXPT]/F_{IPXT}\} \text{ x } V_c/ (V_s \text{ x } T)$$

Where U is the enzyme activity in μmol s^{-1} g $protein^{-1}$, ΔF is the change per second in fluorescence intensity obtained for pterin or methylene blue, [IXPT] is the concentration of the isoxanthopterin (μM) added at the end of the assay. F_{IPXT} is the immediate increase of fluorescence obtained after isoxanthopterin addition. V_c is the final volume used in mL, V_s is the volume of sample added in mL, and T indicate the concentration of the homogenate (mg ml^{-1}).

2.11. Superoxide anion quantification via LECL

For $O_2^{\cdot-}$ quantification via LECL 100 μg protein was added to each well in a 96-well plate, solid white with a flat and transparent bottom (Greiner Bio-One™). Briefly, red phenol-free Hank's Balanced Salt Solution (HBSS, Lonza) supplemented with HEPES (1 mM) pH 7.4 was mixed in a 1:1 v/v ratio with Na_2CO_3/$NaHCO_3$ 0.1 M (4:1 v/v) buffer, pH 11.0; final pH was adjusted with NaOH or HCl 1 M to 10.4. In some cases, protein lysates were incubated with pharmacological inhibitors, febuxostat (1 μM) or DPI (10 μM) for 30 min at 37 °C. Experimental substrate(s) xanthine, NADPH or NADH were added at 100 μM per well, followed by 10 μM lucigenin (Sigma Aldrich, UK) as previous studies [37]. Luminescence was immediately analysed using a PerkinElmer Wallac 1420 Victor 2 plate reader (PerkinElmer, USA), $O_2^{\cdot-}$ anion production was read for 50 repeat readings with 30 s interval between each repeat. Each sample was run in duplicate, and the results averaged to give an n = 1.

2.12. Dihydroethidium (DHE)-determined superoxide anion quantification

For DHE-determined $O_2^{\cdot-}$ quantification 8-well Nunc™ Lab-Tek™ chambered coverglasses (Fisher Scientific) were coated overnight with 300 μl of 1% Gelatin solution in PBS. The solution was then removed and the coverglass air dryed. Following this 120,000 cells were seeded in each well and incubated at 37 °C for 24 h prior to replacement of culture medium with media containing vehicle as control, SOD (600U/ml, Sigma-Aldrich) or $NaNO_2$ (10 μM) for a 2 h treatment period. Following this the media was replaced and DHE/bisBenzamide H 33,342 trihydrochloride (Merk) at a final concentration of 5 μM and 10 μM respectively were added in each chamber for additional 30 min. At the end of the incubation time, the solution was replaced with 200 μl of HBSS (with $Ca^{2+}$and Mg^{2+}) and the fluorescence visualized under a confocal microscope (ZEISS LSM 880 with Airyrscan) equipped with an Apochromat 63 × ; 1.4 numerical aperture (NA) oil objective (Zeiss, Germany)). Images analysed with Image J Software (Fiji, NIH). For each mutant, 18 images were randomly taken based on the presence of a minimum of 15 cells per field. The mean intensity, area and integrated density were measured for both Hoechst 33,342 and DHE. DHE integrated density was normalised to the area of Hoechst. The DHE/Hoechst ratio per mutant was then normalised to XOR expression measured by immunoblotting from aliquots of the same cell preparations.

2.13. UA quantification

1.3×10^6 cells were seeded into 75 cm^2 flasks. After 72 h the medium was replaced and supplemented with xanthine 20 μM or 100 μM and incubated at 37 °C for 3 h, after which cell pellets were collected as above, and stored at −80 °C for future assessment. One half was used for protein extraction and the other half used for UA quantification using a UA Assay Kit (MAK077, Sigma-Aldrich). Cells were disrupted mechanically, and the sample centrifuged at 15,871 RCF at 4 °C. The supernatant was then added to a 96-well plate for colorimetric quantification using a spectrophotometer at 570 nm. UA values were obtained by interpolation from a standard curve and then normalised to the protein concentration.

2.14. NO_2^--reductase assessment

NO_2^--reductase activity was measured in cell lysate using gas-phase chemiluminescence as previously described [38]. Cell pellets were homogenised with homogenization buffer devoid of Triton X-100. Prior to use for NO_2^- reductase assessment protein concentration was determined. Experiments were performed in a sealed 10 ml glass reaction chamber containing citric acid/sodium phosphate dibasic (Na_2HPO_4) (Sigma Aldrich) buffer at pH 6.8 (representing acidosis), and $NaNO_2$ (10–1000 μM) in a total volume of 1 ml. This solution was bubbled with nitrogen gas (100%) via an ·NO scrubbing air filter (Sievers, USA) to eliminate all O_2. Headspace ·NO concentration was measured in parts per billion by continuous sampling using a 280 A ·NO Analyzer (Sievers, USA). In all experiments a baseline NO signal (in ppb s^{-1}) was obtained for 3 min followed by addition of the protein sample (250 μg) and then after a further 10s the addition of $NaNO_2$. To compare the impact of

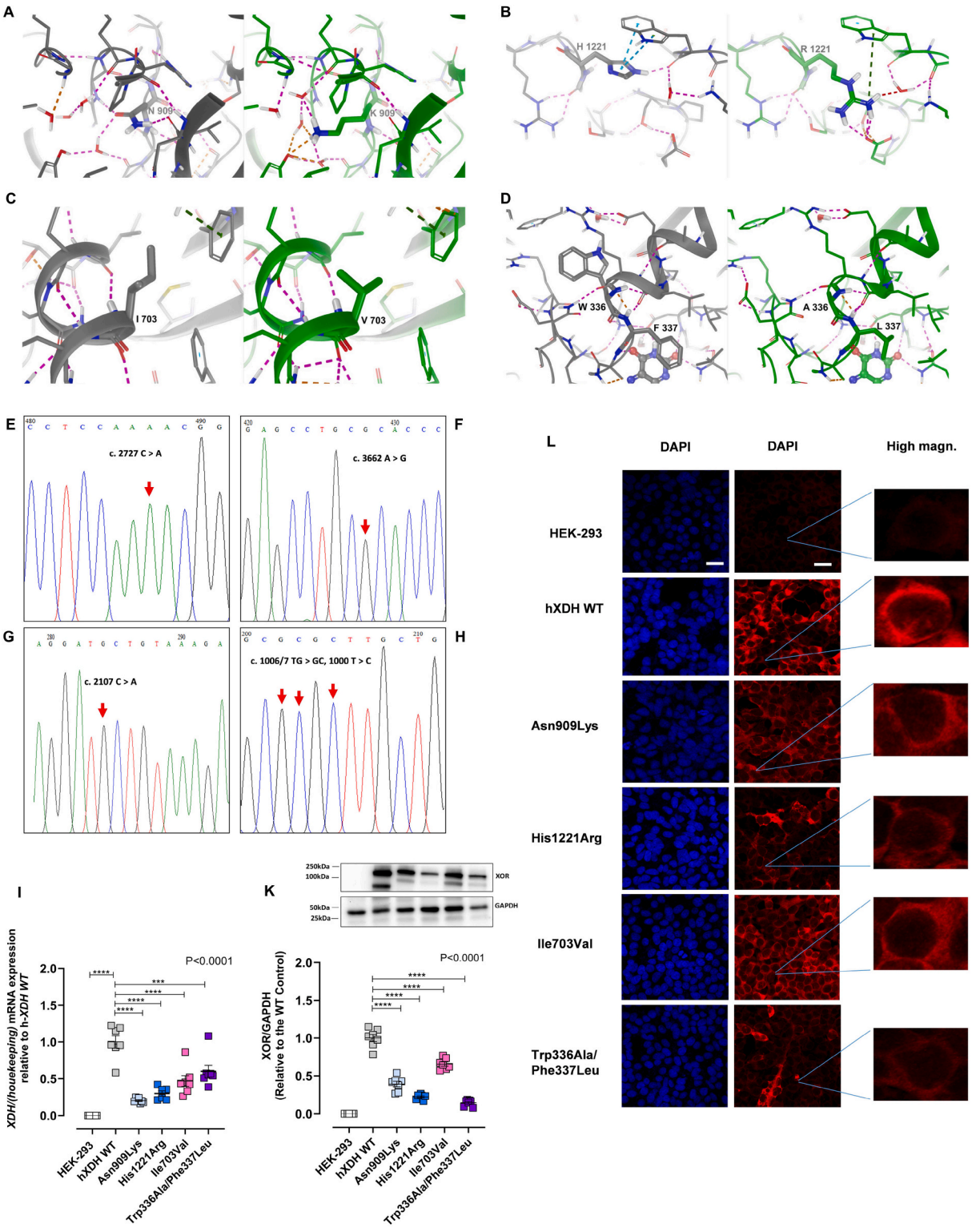

Fig. 1. Impact of *hXDH* mutations on XOR protein structure and expression. Wild type structure (2E1Q) is shown in grey beside the mutated structure shown in green. Residues within 5 Å of the mutated residue are shown as thin sticks, whilst the mutated residue is shown as thick sticks. Interactions are indicated by dashed lines, with H-bonds in magenta, aromatic in cyan, cation-pi in dark green, with other non-bonded short contacts shown in orange or red according to increasing severity. A) N909K, B) H1221R, C) I703V and D) W336A/F337L.

Figure also shows sanger sequencing chromatograms of site-specific mutation sourced in the pEGFP-N1 plasmid vector are shown for E) 2727 C>A leading to Asn909Lys mutation, F) 3662 A>G accounting for His1221Arg, G) 2107 A>G leading to Ile703Val, H) triple mutation 1006/7 TG>GC + 1009 T>C leading to the Trp336Ala/Phe337Leu. I) shows mRNA levels (n = 7) of the various mutants versus the WT and K) representative immunoblotting (n = 7) and its quantification of WT and mutated hXOR. GAPDH has been used for protein normalization. L) shows XOR expression detected via immunocytochemistry with DAPI (blue), XOR (red). Magnification ×40; scale bar 30 μm. All data are expressed as mean ± SEM of data and compared using one-way ANOVA with Dunnett post hoc analysis comparing to the hXDH WT control. Post-test significance shown as ***p < 0.001, ****p < 0.0001. (For interpretation of the references to color in this figure legend, the reader is referred to the Web version of this article.)

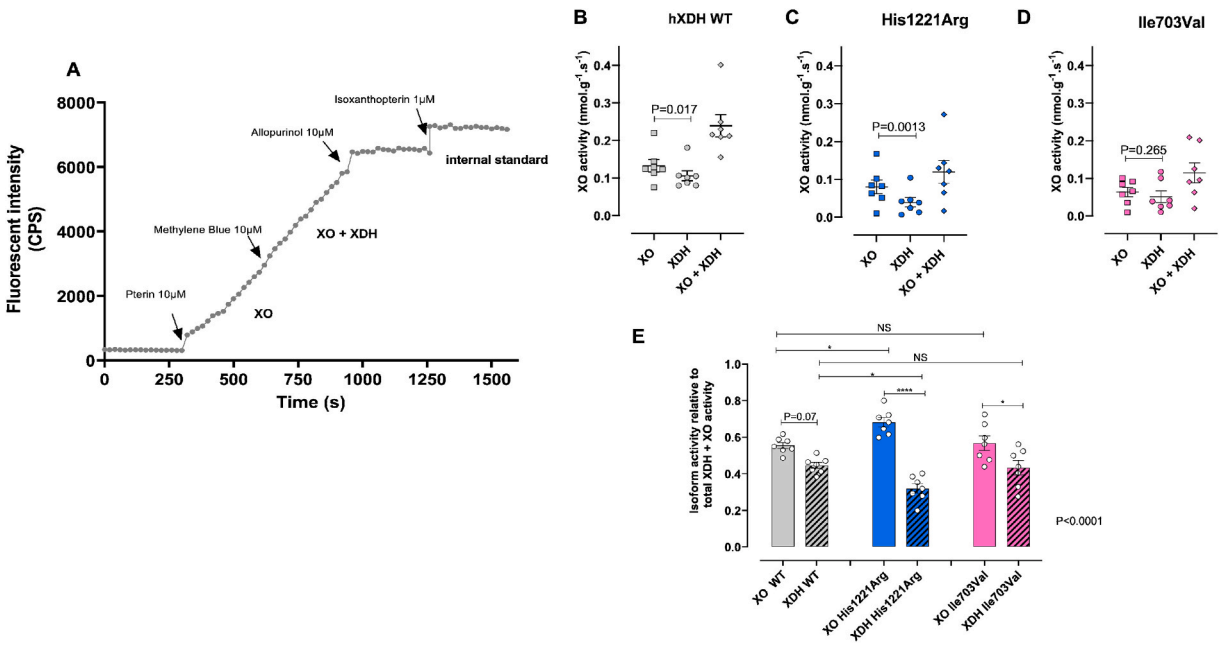

Fig. 2. Genetic mutations influence XDH conversion to XO. Panel A) shows a representative trace of XO and XDH+XO fluorometric activity in the presence of pterin and methylene blue respectively over 300s intervals of recording. Panels (B–D) show the absolute activity of XO, XDH, and XO + XDH in hXDH WT, His1221Arg, and Ile703Val. Figure E) shows the XO and XDH activity relative to total XO + XDH activity (n = 7). Pterin, methylene blue, allopurinol were used at a final concentration of 10 μM, whereas isoxanthopterin, the internal standard, was used at 1μM final concentration. Fluorescence was recorded every 20 seconds for 5 minutes. Data are expressed as mean ± SEM of data and compared using a paired *t*-test comparing XO and XDH activity for B–D. For E statistical significance was determined using one-way ANOVA (P value in right hand corner) with Sidaks post-test comparing XO and XDH activity for each genotype and XO WT versus XO activity of each mutation and XDH WT versus XDH of each mutation, with adjusted post-test significance accounting for multiple comparisons shown (For interpretation of the references to color in this figure legend, the reader is referred to the Web version of this article.)

distinct mutations to the WT the average rate (ppb s^{-1}) chemiluminescent signal of ·NO over 3 min was converted to mol s −1 and expressed relative to g protein using the following formula:

$$\text{NO rate} = \text{ppb x}(0.0038\ \text{L s}^{-1}/24.47\text{L})\times 10^{-9}\ \text{x g}^{-1}$$

The NO analyzer samples at a rate of 0.0038 L per second. Since 24.47 L is the volume of 1 mol of ideal gas under standard conditions (25 °C and 1 atm) the ppb values were converted to moles using these inferences and expressed relative to protein present. To confirm involvement of XOR, protein samples were pre-treated with febuxostat (10 μM) or vehicle control (0.05% DMSO) for 30 min. Furthermore, to establish whether non-synonymous mutations influenced the enzyme selectivity toward Mo–Pt or FAD reducing agents and consequently the NO_2^--reductase activity, nitrite-reductase activity was carried out in presence of xanthine (20 μM) and NADH (100 μM).

2.15. Statistical analysis

Statistical analysis was conducted using GraphPad Prism 9 software. All data are expressed as mean ± SEM. For statistical comparison, either an unpaired student *t*-test analysis or one-way ANOVA with Dunnett's post hoc analysis, or two-way ANOVA followed by Dunnett or Sidak's post hoc analysis for multiple group comparison were used as appropriate. Any *P* value less than 0.05 was used to infer significance. For all datasets an n = 7 was achieved. Where the n value is less than this is due to technical failure. The n value of 7 was set according to our preliminary experimental findings with assessment of superoxide levels in control untransfected cells and those transfected with our preliminary data with 5 independent experiments (separate cultures conducted on different days of the source cells) and demonstrated that cell homogenate incubated with Xanthine (100 μM) gave an average count per second (CPS) of 146 (SD = 14) and *hXDH* transfected cells gave 440 (SD = 38). Thus, with an α = 0.05 and a power of 95% an n = 5 independent experiments are required to observe statistical differences. To account for potential technical failure, we increased this number to 7.

3. Results

3.1. Computational analysis of 3D structure of mutated XDH

To explore the impact of *hXDH* mutations upon enzyme function we first assessed four well described *hXDH* mutations upon the predicted structure of the protein; namely Trp336Ala/Phe337Leu, Ile703Val, His1221Arg and Asn909Lys (Table 1, Fig. 1A–D) [27,34]. Importantly, these mutations occur naturally within the human population except for the Trp336Ala/Phe337Leu, which was created experimentally and selected specifically due to its localisation at the FAD site of the enzyme [34].

The 2EIQ structure, which is a 2.6 Å resolution of the full-length human structure already contains a mutation (E803V) at the Mo–Pt site which is known to affect function, however this does not impact the structure in any way based on comparison with 2CKJ. Residues 164–191 are not visible in the density, nor are they in the other human structure 2CKJ. Given that this loop is exposed, long and flexible any predicted conformation would be of low reliability, so we did not pursue to build this part of the protein. Fig. 1 (A-D) shows the predicted structures of the protein in presence of the mutations assessed. N909 is largely buried, but not too tightly enclosed. Interactions between its sidechain and the peptide backbone are lost on mutation to lysine and adjustment of the solvent network observed in the crystal is also required to accommodate the change. H1221 interacts with the backbone and sidechain of W1329, likely stabilising the loop structures in this region. Mutation to arginine is a substantial change and whilst the aromatic interactions with W1329 are lost, there are still some interactions due to the cationic nature of the arginine, which also engages with E1217. I703 is engaged in hydrophobic interactions with F865, F708 and I699, helping to stabilise

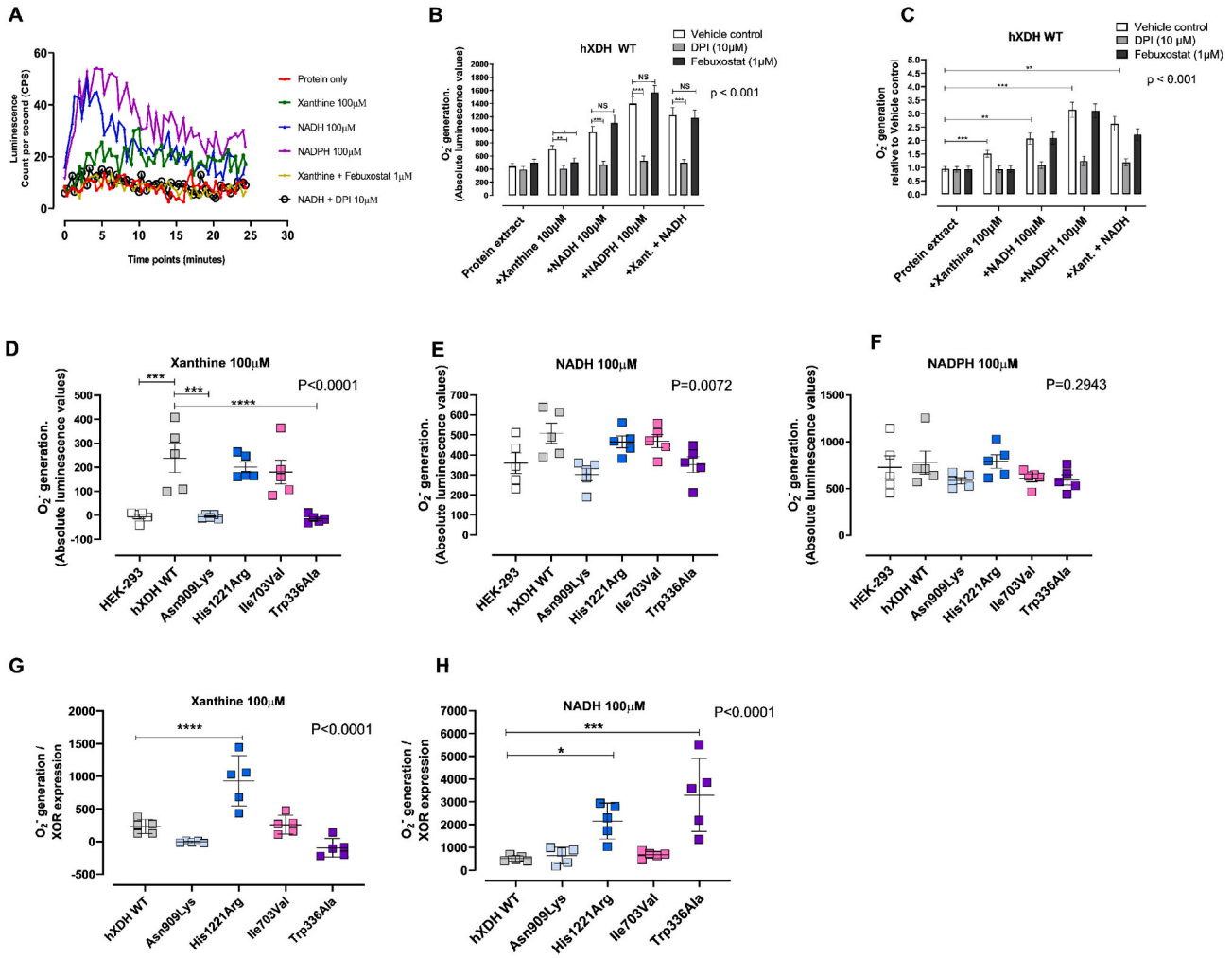

Fig. 3. Impact of *hXDH* mutations upon superoxide anion ($O_2^{\cdot-}$) generation. Panel (A) shows representative traces of $O_2^{\cdot-}$ quantification over 25 min of reading via lucigenin-enhanced chemiluminescence reaction (LECL) in the presence of 100 μg of cell lysate of WT and mutated *hXDH* cell lines in the absence and presence of Mo–Pt-reducing substrate Xanthine (100 μM), FAD-reducing substrate NADH (100 μM), and NADPH oxidase-specific substrate NADPH (100 μM). Panels (B–C) show $O_2^{\cdot-}$ generation (n = 7) over 25 min in the absence and presence of a Mo-specific inhibitor, febuxostat (1 μM), and FAD inhibitor diphenyleniodonium (10 μM) in HEK-293 and *hXDH* WT stable cell lines respectively. Panel (D–F) show $O_2^{\cdot-}$ quantification (n = 5) in presence of xanthine (D), NADH (E) and NADPH (F). Finally, $O_2^{\cdot-}$ quantification normalised to XOR expression level are shown for the cell lines in the presence of xanthine (G) and NADH (H). Data are presented as mean ± SEM. Statistical difference between groups was measured using two-way ANOVA for B and C with post-tests comparing each vehicle control response to the response in either DPI or febuxostat treated samples. For D-H one-way ANOVA followed by Dunnett's post hoc analysis comparing to the hXDH WT control was conducted with post-test significance shown as × for $p < 0.05$, *** for $P < 0.001$ and **** for $P < 0.0001$.

packing of the helix against the beta sheet. Mutation to valine is quite conservative but reduces hydrophobic contact. W336 is tightly enclosed and loss of packing interactions on mutation to alanine is expected to destabilise interactions in this region possibly resulting in conformational perturbations beyond those reflected in the modelled structure.

3.2. Characterization of hXDH WT and mutant cell lines: sanger sequencing chromatograms, mRNA quantification and XOR expression level

Sanger sequencing confirmed WT and mutant sequences as expected (Fig. 1*E*–H). qPCR analysis revealed a significant difference of XDH mRNA and protein expression levels across the cell lines, with WT showing an mRNA level 2.0-fold higher than Trp336Ala/Phe337Leu, 2.5-fold when compared to Ile703Val, 3.4-fold higher than His1221Arg, and 5.0-fold when compared to Asn909Lys ($P < 0.0001$, Fig. 1I). Immunoblotting revealed the presence of two bands, as described previously, attributed to XDH and XO [39,40], at ~150 and ~100 kDa respectively. For quantification the band for the intact protein at 150 kDa was used, although inclusion of the second band does not alter the pattern of expression. The analysis confirmed a significantly higher expression of XOR WT protein compared to the variants. Interestingly, for Trp336Ala/Phe337Leu we observed a lower level of protein than mRNA detection intimating perhaps that the mutation exerts a negative impact on the maturation or stability of the protein. In contrast, for Asn909Lys the opposite effect was observed (Fig. 1K). The protein expression levels were confirmed by confocal microscopy (Fig. 1L) and flow cytometry (Fig. S1). Magnification of the images from the confocal assessments identified similar localisation of the WT and mutant proteins largely within the cytoplasm (Fig. 1L). Total protein concentrations of collected cell lysates across the distinct cell lines were similar, except for Trp336Ala/Phe337Leu (23.05 μg/μl) which produced higher levels than HEK cells alone (17.44 μg/μl).

Since the mutations exerted a differential impact upon XOR protein expression, comparisons between mutants were made both before and after normalization to XOR expression levels in the same lysate determined using 50 μg of cell lysate for immunoblotting detection. This amount of cell lysate protein was used for this since it provided an

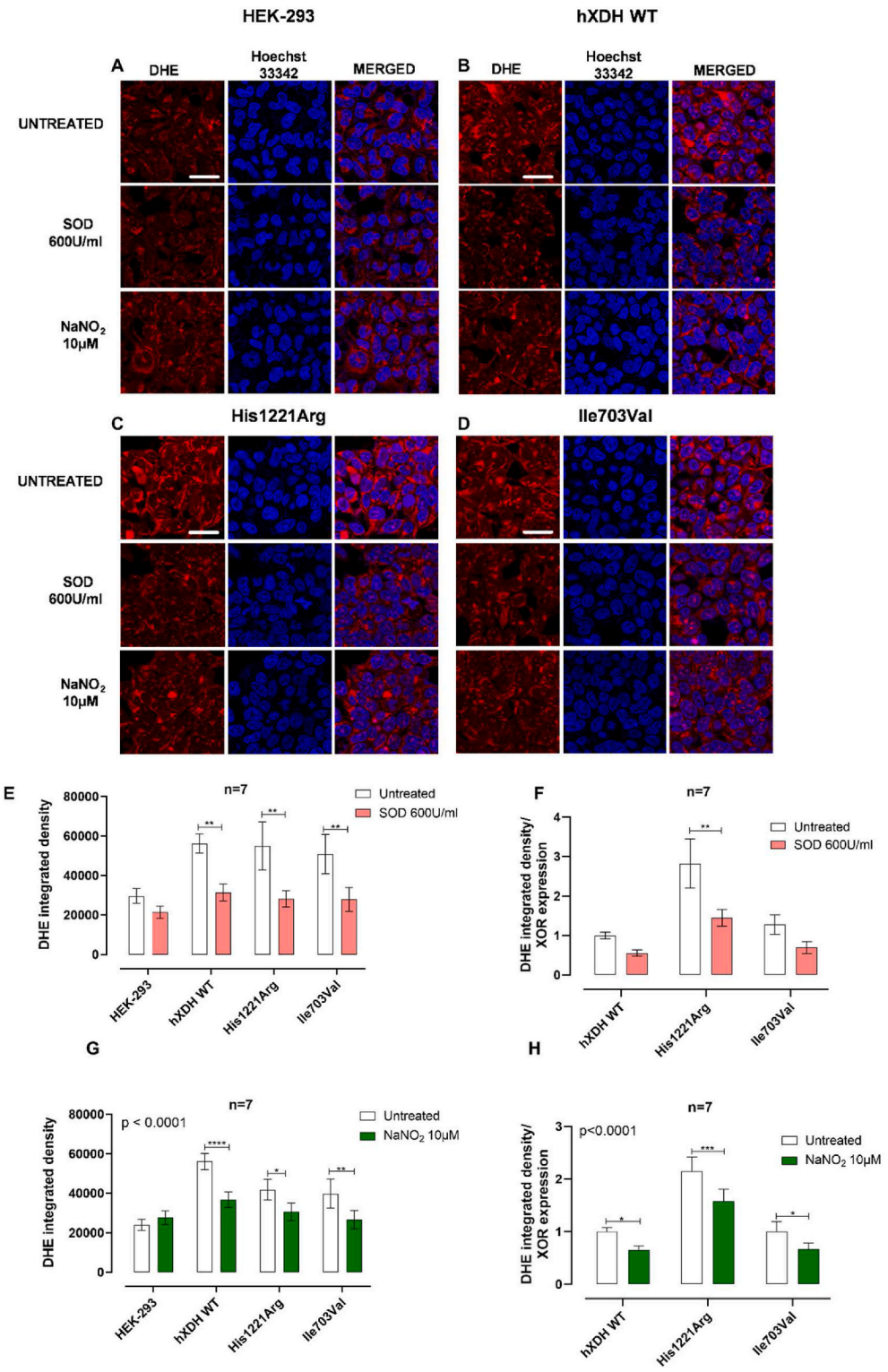

Fig. 4. Superoxide dismutase (SOD) and inorganic $NaNO_2$ decrease O_2^- levels. Panels A–D) show representative superoxide anion (O_2^-) quantification (n = 7) via immunocytochemistry with DHE (red) and Hoechst (blue) in HEK-293, in hXDH WT, His1221ARg and Ile703Val respectively. E-F) show O_2^- quantification in presence of superoxide dismutase (SOD) (600U/mL) before and after normalization to XOR expression respectively; G-H) show O_2^- quantification (n = 7) in presence of $NaNO_2$ (10 μM) before and after normalization to XOR expression respectively. N values are shown on the graphs. Magnification ×40; scale bar 30 μm. All data are expressed as mean ± SEM of data and compared using Two-way Anova with SidaK post hoc analysis. *p < 0.05, **p < 0.005, ***p < 0.0005, ****p < 0.0001. (For interpretation of the references to color in this figure legend, the reader is referred to the Web version of this article.)

indication of XOR within the linear phase of expression (Figs. S2A and B).

3.3. Genetic variants of hXDH influence the XO:XDH activity relationship

The proportions of XDH (54%) and XO (46%) activity of the WT relative to total pterin oxidation activity (0.2389 ± 0.01 nmol/g/s, n = 7) revealed statistically significant differences in the oxidative and dehydrogenase activities of the distinct mutations (Fig. 2B–D). In untransfected HEK-293 cells, total XDH + XO activity was negligible (0.0012 ± 0.0008 nmol/g/s, n = 6). The Asn909Lys (XDH + XO = −0.0005 ± 0.0004 nmol/g/s) and Trp336Ala/Phe337Leu (−0.00008 ± 0.0009 nmol/g/s) mutations eliminated all activity of the enzyme in this assay. The non-synonymous mutation His1221Arg showed a similar total activity as that of h*XDH* WT, however the proportion of XO activity was substantially greater than that seen in the WT (~70%, Fig. 2E) suggesting a potential pro-oxidative effect of the mutation. When normalised to total XO/XDH activity the level of XO activity for Ile703Val

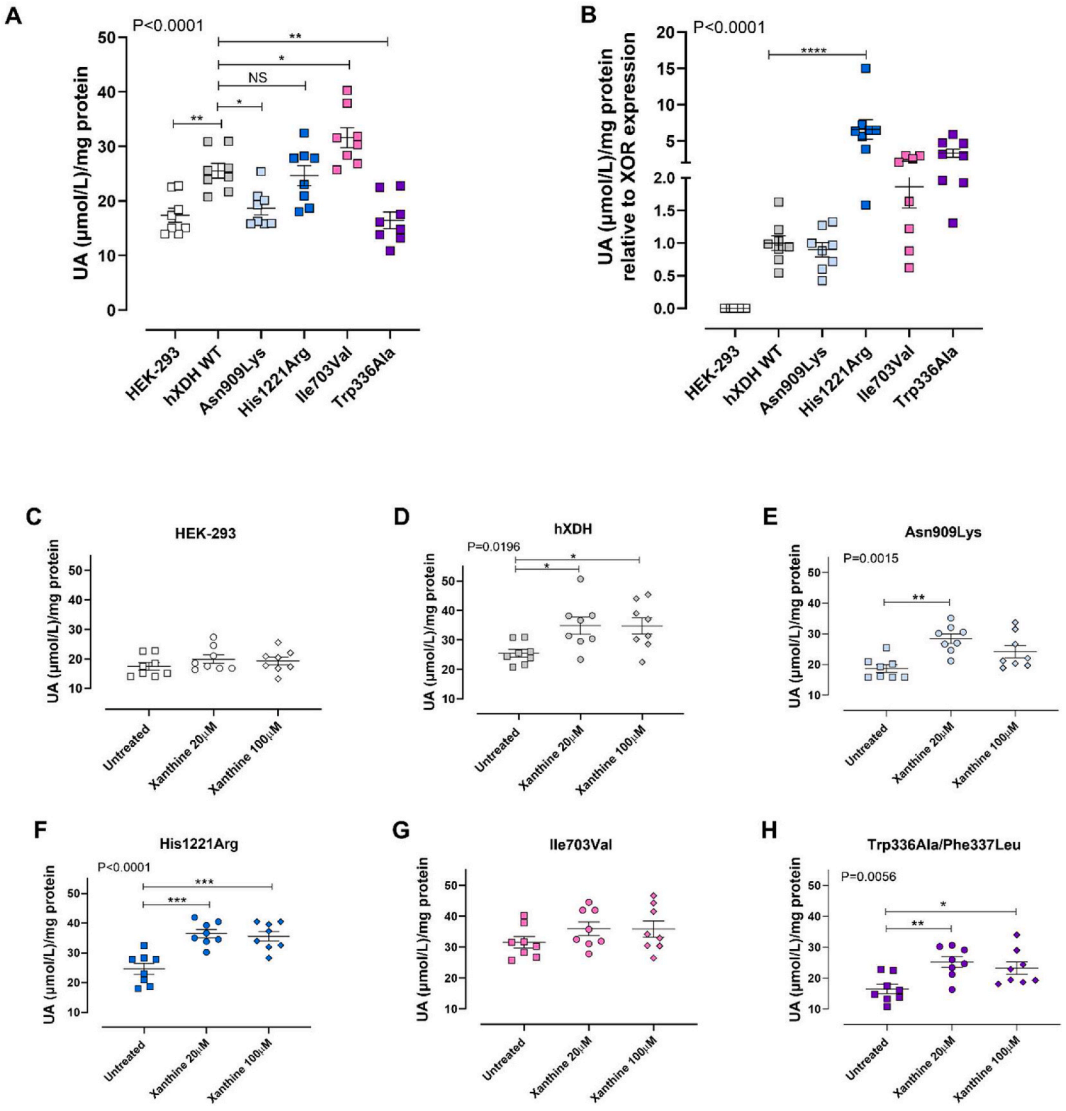

Fig. 5. Mutations in XOR influence uric acid (UA) production. Panel (A) shows UA levels in the XDH WT and mutant cell lines at baseline relative to total protein concentration or following normalization to XOR expression (B) determined by Western blotting of the same sample. Panels C–H show the absolute UA levels generated from 4×10^6 million cells incubated with xanthine 20–100 μM. Data are shown as mean ± SEM. Statistical analysis was conducted using one-way ANOVA with Dunnett's post-hoc analysis for comparison to hXDH WT of n = 8 independent experiments. *for $p < 0.05$, **for $P < 0.005$, ***$P < 0.001$ and **** for $P < 0.0001$.

was also statistically significantly higher than the XDH proportions (Fig. 3D and E).

3.4. $O_2^{\cdot-}$ production is influenced by genetic variations

His1221Arg and Ile703Val, statistically significantly increased O_2 reduction compared to HEK-293. On the contrary, the *C*-terminal non-synonymous mutation, Asn909Lys, and the double mutation Trp336Ala/Phe337Leu, showed no residual oxidase activity implying a plausible conformational alteration of the tertiary structure around the Mo–Pt site (Fig. 3). Confirmation of XOR and FAD site involvement in xanthine-driven $O_2^{\cdot-}$ generation in this assay, was demonstrated by block of the response with febuxostat and DPI respectively (Fig. 3B and C). As expected, whilst both inhibitors blocked xanthine driven $O_2^{\cdot-}$ generation in WT, only DPI blocked NADH or NADPH driven radical generation. Of note, febuxostat caused an elevation of $O_2^{\cdot-}$ generation in the presence of both these substrates although this did not reach statistical significance. To confirm that XOR overexpression did not influence NADPH oxidase expression and activity we also exposed our cell lines to NADPH. As expected, NADPH oxidase activity was not affected by the over-expression of XOR with the $O_2^{\cdot-}$ quantification consistent throughout the mutations (Fig. 4F). Since the mutations exerted a differential impact upon protein expression, $O_2^{\cdot-}$ measurements were normalised to XOR expression level estimated from the same lysates using Western blotting analyses. This normalization demonstrated that His1221Arg mutation resulted in a significantly higher $O_2^{\cdot-}$ production compared to hXDH WT in the presence of either xanthine or NADH (Fig. 4G and H) whilst the other mutations showed no statistical difference in oxidase activity to h*XDH* WT in the presence of xanthine. Although most trended to be lower particularly Asn909Lys and Trp336Ala/Phe337Leu ($p = 0.07$) and, in the presence of NADH, Trp336Ala/Phe337Leu and His1221Arg showed increased activity relative to WT (Fig. 4H).

We validated the observations obtained with the lucigenin assay by measuring ROS production using the DHE fluorogenic probe. Similarly, to the findings with the lucigenin protocol, cells expressing hXDH WT, His1221Arg, or Ile703Val mutants have raised DHE-fluorescence compared to untransfected HEK-293 (Fig. 4A–F) indicating increased $O_2^{\cdot-}$ levels. Treatment with SOD reduced DHE fluorescence in all mutants

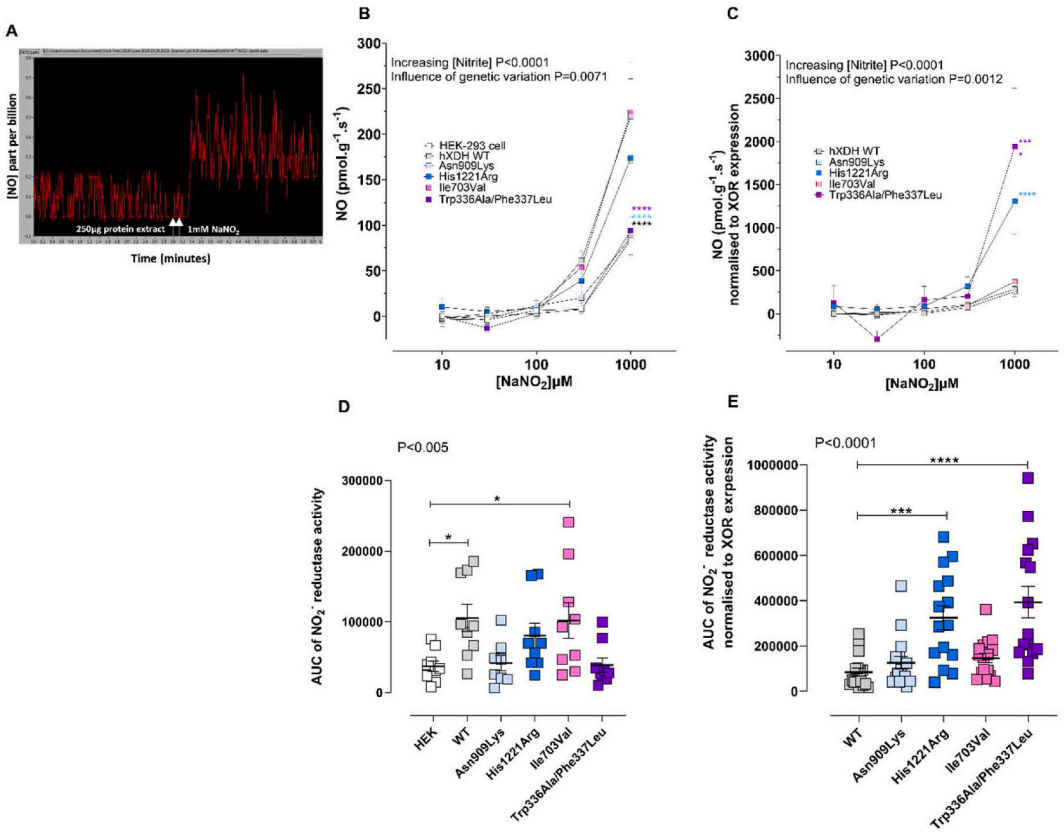

Fig. 6. The effects of genetic variation on the NO_2^--reductase activity of XDH. Panel (A) shows a typical trace of NO production; B) shows the NO_2^--reductase activity measured using ozone chemiluminescence with 250 µg of cell lysate of untransfected HEK and hXDH WT, Asn909Lys, His1221Arg, Ile703Val, and Trp336Ala/Phe337Leu expressing HEK cells. Panel (C) shows the ·NO generation following normalization to XOR expression levels of the same samples. Panels (D–E) show the AUC of the baseline NO_2^--reductase activity. Data are shown as mean ± SEM of n = 9 independent experiments. Statistical analysis conducted using two-way ANOVA comparing all curves to the hXDH WT control with *P*-values shown for the variables and post-hoc comparisons at each concentration determined using Sidak's post-hoc test and one way ANOVA with Dunnett's post-hoc comparisons for comparison to HEK-293 (C) or hXDH WT (D) and shown as × for $P < 0.05$, ***for $P < 0.001$ and **** for $P < 0.0001$.

to levels comparable to untransfected HEK-293 (Fig. 4A–E), confirming the specificity of the assay in detecting O_2^--dependent oxidation. Normalising to XOR expression the O_2^- generating capacity of the variants versus the WT were similar in both methods. Using the DHE-based method we confirmed the specificity for O_2^- since incubation with SOD substantially reduced the signal relative to the untransfected HEK-293 (Fig. 4F,H).

3.5. *Differences in the genetic sequence alter UA production either in presence or absence of xanthine*

To explore the impact of the mutations upon activity of the enzyme at the Mo–Co site we measured UA synthesis. As expected, baseline levels of UA were elevated in hXDH WT versus untransfected HEK-293 controls (Fig. 5A). His1221Arg and Ile703Val exhibited significantly increased levels of UA when compared to untransfected controls, with Ile703Val resulting in higher levels than hXDH WT (Fig. 5A). To compare enzyme activity between variants more closely we normalised UA values to XOR expression levels. This revealed that only the His1221Arg mutation, in line with previous observations, was associated with a statistically significant raised urate level compared to hXDH WT (Fig. 5B). Surprisingly, despite elimination of all O_2^- generating activity UA levels were unchanged compared to WT with the Asn909Lys mutation. These results suggest that this non-synonymous substitution did not alter the active site cavity at the Mo–Co domain in a manner that prevented access and binding of xanthine. The double mutation isoform Trp336Ala/Phe337Leu increased UA levels compared to the WT but this did not achieve statistical significance (Fig. 5B). Exposure of each cell line to xanthine demonstrated concentration dependent elevations for all mutations whilst untransfected cells did not respond (Fig. 5C–H).

3.6. *Improved NO_2^- reductase activity of specific hXDH mutants*

We next explored whether specific hXDH mutant forms might influence the NO_2^--reductase capacity and so the generation of the beneficial molecule ·NO. The expression of hXDH WT in HEK-293 led to an increase in NO_2^- -reductase activity above that with untransfected HEK-293 control. This elevation was also evident with both the His1221Arg and Ile703Val mutants (Fig. 6A). Interestingly, both mutants Asn909Lys and Trp336Ala/Phe337Leu did not appear to show any differences in terms of absolute ·NO formation in comparison to untransfected cells (Fig. 6A). When the NO_2^--reductase activity was normalised to XOR expression level, His1221Arg exhibited an overall statistically significant higher NO_2^--reductase activity compared with the hXDH WT (Fig. 6B) with a slight trend for elevation with Asn909Lys and also Ile703Val at baseline and in the presence of reducing substrate confirming a general trend for increase with all of the mutations despite clear differences in the O_2^- generating activities of these mutations (Fig. 6C and D). Interestingly, whilst febuxostat prevented the activity for most mutations it did not impact activity in cells expressing Asn909Lys and Trp336Ala/Phe337Leu (Fig. 7). Importantly, using DHE-based confocal studies $NaNO_2$ substantially reduced O_2^- levels in cell lysates from WT, His1221Arg and Ile703Val mutants but not in untransfected HEK-293 controls (Fig. 4G and H). These finds suggest

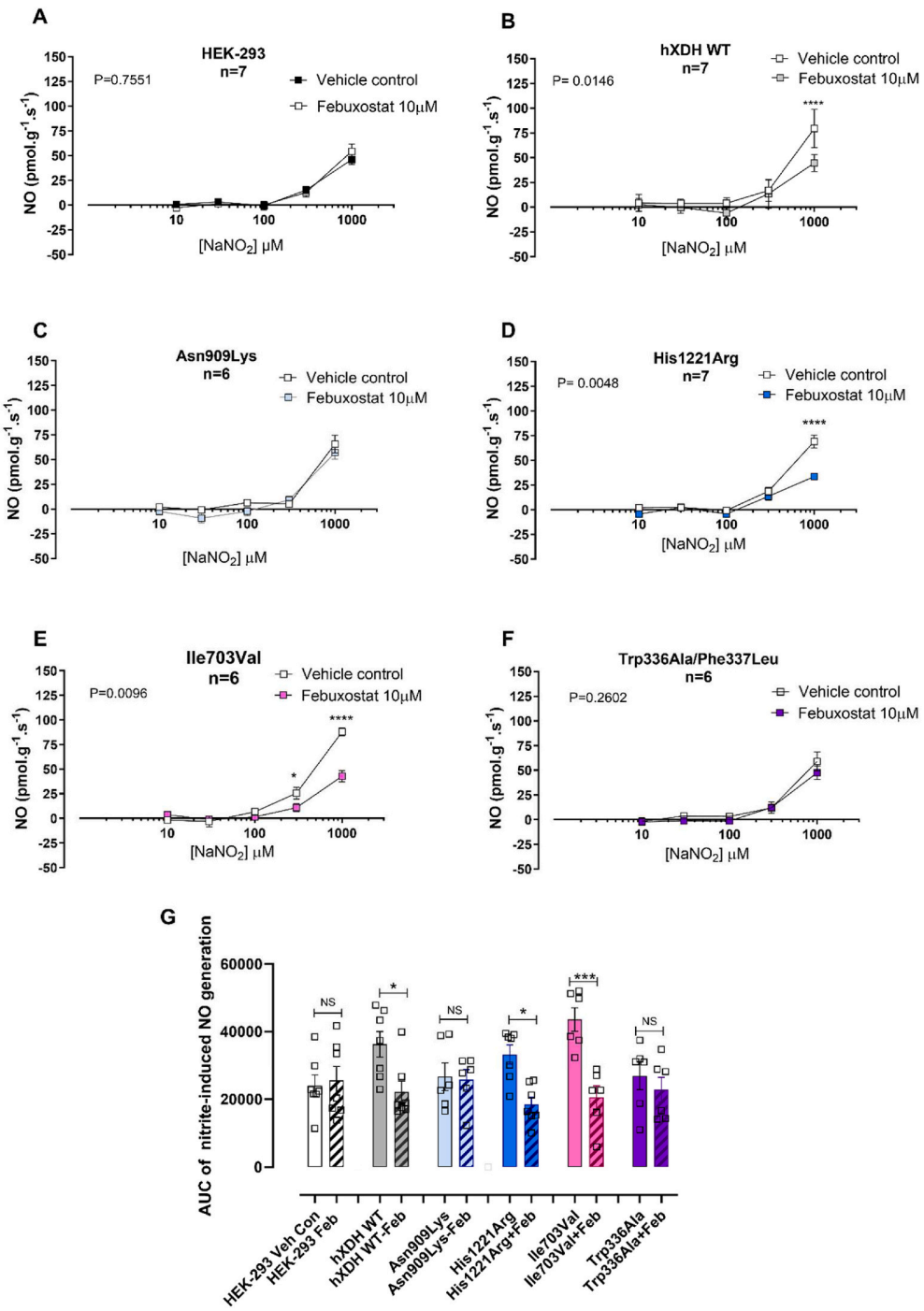

Fig. 7. The XOR inhibitor Febuxostat (10 μM) prevents NO_2^-–reductase activity. Figure A–F show the nitrite-reductase activity (n = 7) in presence of a Mo–Pt specific inhibitor, febuxostat (10 μM), and G) shows the AUC of NO_2^--reduction ·NO generation. Statistical analysis conducted using two way ANOVA comparing vehicle vs febuxostat 10 μM with *P*-values shown for the variables and post-hoc comparisons at each concentration determined using Sidak's post-hoc test (A–F) or one way ANOVA followed by Sidak's post-hoc test for multiple comparison test (G) and shown as × for $P < 0.05$, ***$P < 0.005$, and **** for $P < 0.0001$.

competition for electrons between the Mo–Co and FAD sites of the enzyme that is pushed in favour of the Mo–Co with increasing concentrations of NO_2^-.

3.7. Xanthine and NADH increase NO_2^--reductase activity

Since XOR catalyses the one electron reduction of NO_2^- to ·NO in the presence of either xanthine or NADH [41] we measured ·NO formation in the presence of optimal concentrations of each substrate. Interestingly, only the WT and those cells expressing the Ile703Val mutation demonstrated an increase in activity versus the vehicle control in the presence of either substrate (Fig. 8). Interestingly, whilst xanthine increased NO_2^- reduction in cells expressing the His1221Arg mutation, no statistically significant effect of NADH was demonstrated (Fig. 8G and H).

4. Discussion

There has been considerable interest in identifying genetic variants of *XDH* that might associate with disease. This is particularly due to the strong associations of disease outcomes with products of XOR activity, most commonly UA for gout, metabolic syndrome, and CVD; the latter including hypertension and coronary artery disease. It is notable however, that of the known mutations that exist for the h*XDH* gene, the majority are rare and have been functionally associated with the equally uncommon phenotype of xanthinuria [19,25,28,42,43]. In addition,

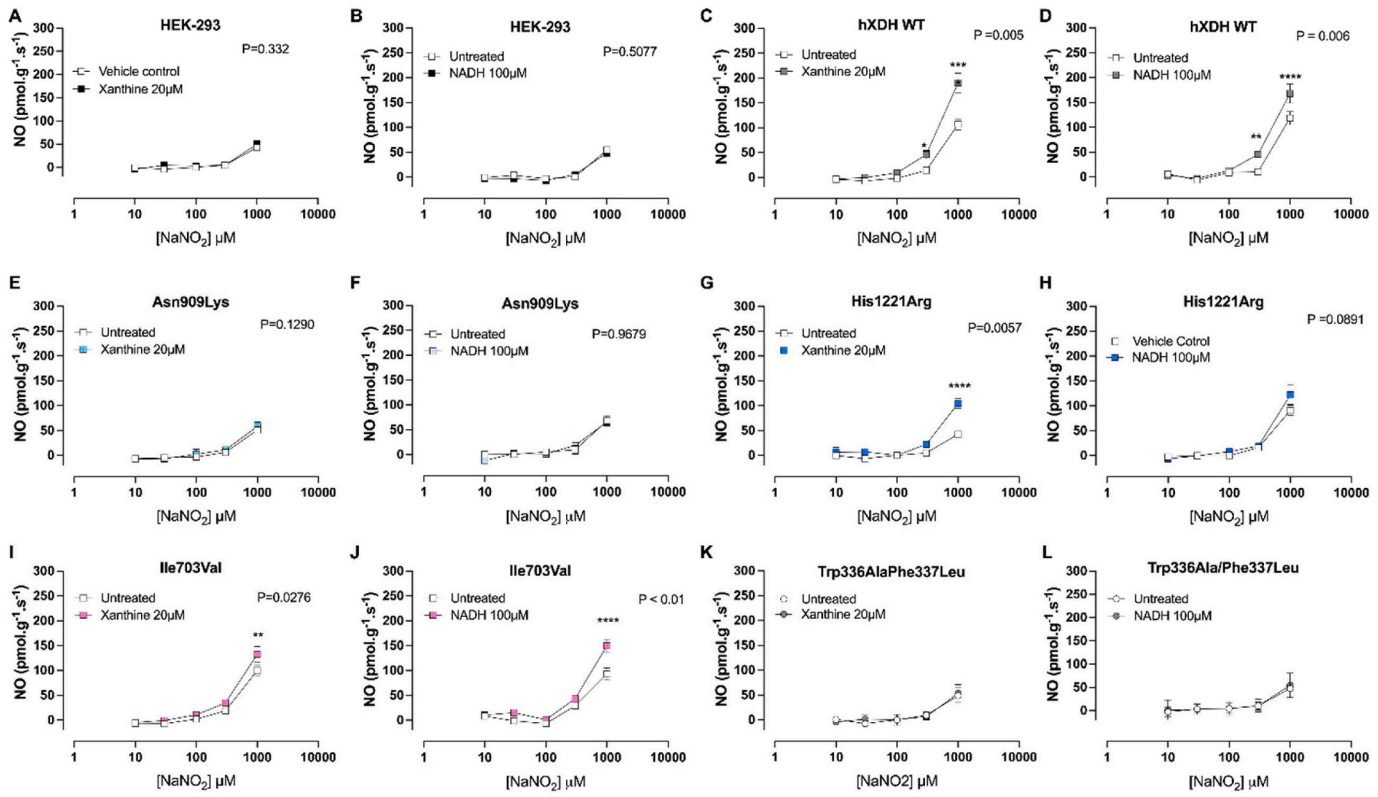

Fig. 8. Xanthine and NADH increase NO_2^--reductase in hXDH wild type, His1221Arg and Ile703Val expressing cells. The panels show NO_2^--reductase activity measured by ozone chemiluminescence using 250 μg of cell lysate in presence of XOR reducing agents, xanthine 20 μM or NADH 100 μM respectively, in HEK-293 cells (A–B), hXDH WT (C–D), Asn909Lys (E–F), His1221Arg (G–H), Ile703Val (I–J) and Trp336Ala/Phe337Leu (K–L). Data are shown as mean ± SEM of n = 6–8. Statistical analysis conducted using two-way ANOVA with Sidak's post-hoc comparisons between the treatments and shown as **P < 0.01 and **** as P < 0.0001.

there is a growing equipoise regarding the clinical utility of targeting the enzyme for the treatment of disease beyond gout [10]. We assessed the biochemical activity of some well-described mutations from the literature that have been associated with xanthinuria or increased UA synthesis and combined this with assessment of the previously unconsidered NO_2^--reductase activity of the variant. Herein, we show that previously identified SNPs may have an impact on mRNA stability with direct consequences on XOR expression levels and activity. We also show that non-synonymous substitutions within the peptide chain affect the XDH/XO proportion and consequently its oxidase activity as well as its affinity for the final electron acceptor, NAD^+ or O_2, with direct consequences for UA, ROS production and NO_2^--reductase activity. Our findings demonstrate important unexpected impacts upon NO_2^--reductase activity of mutations known to occur in the population that theoretically might improve the redox balance in vivo and so potentially health status. Finally, we demonstrate that, by simply providing inorganic $NO_2^{\cdot}$ which competes for electrons at the Mo–Pt domain, that XOR activity can be switched from detrimental to beneficial due to lower O_2^- production and higher ·NO release. Whilst not tested in this study, recent evidence also suggests that enhanced NO_2^- reduction in patients with CVD was associated with lowering of UA levels [17]. Considering these observations, we suggest that reassessment of both common and rare SNPs in XOR should be explored to include determination of the impact upon NO_2^--reductase activity.

XOR is considered to express a subcellular localisation predominantly within the cytoplasm [44] but also on the outer surface of the cell membrane [45]. Rouquette et al. also demonstrated a polarised distribution on the cell surface in regions of close cell-to-cell contact. The confocal studies herein also demonstrate cytoplasmic expression. It is noteworthy that this cellular distribution was largely unchanged for each of the mutants indicating that any differences between the mutants does not relate to differences in cellular localisation. However, substantial differences in mRNA expression levels of the mutations versus the h*XDH* WT that was not directly matched to protein expression was observed. This observation is in line with previous findings demonstrating that exonic point mutations may influence mRNA levels by altering its stability [46]. It is also possible that the observed changes in gene expression result from variations in the integration process of the external gene within the host genome. However, this is unlikely since the protocols used for each mutation and the host cell source for the expression were identical. The disconnect between mRNA and protein expression was most pronounced for the two mutations Trp336Ala/-Phe337Leu and Asn909Lys. Importantly, whilst the former exhibited a diminished level of XOR protein compared to the detected mRNA, suggesting a negative impact of the double mutations on the maturation or stability of the protein, the opposite was observed with the latter. These observations are similar to previous findings in COS-7 cells, transiently transfected with human *XDH*, where differential protein expression levels across the investigated mutants was evidenced [27]. Interestingly, in this study in COS-7 cells the Mo–Co mutation Asn909Lys, almost eliminated detectable protein. This contrasting observation may relate to the experimental approach used or it may suggest a cell-specific expression effect. Indeed, in support of this observation a study published by Kudo et al. [33] demonstrated that the luciferase reporter assay, used to evaluate whether mutations within the promoter region of *XDH* have an effect upon XOR expression, revealed significant differences between investigated SNPs as well as different cell lines.

Numerous pathological stimuli including pro-inflammatory cytokines [47–49], unhealthy diet [50], cigarette smoke [51], hypoxia [52, 53], ischemia-reperfusion injury and CVD risk factors (such as hypertension [54]) increase XOR expression and activity. These stimuli also promote the conversion of XOR from the housekeeping reduced isoform,

Table 2
Summary table indicating fold changes of hXDH mutants relative to XDH WT.

Mutation	Gene and protein expression		XDH and XO pterin proportion		$O_2^{\cdot-}$ generation		UA	NO_2^- -reductase activity
	XDH mRNA	XDH protein	XDH	XO	Xanthine	NADH		
hXDH WT	1±0.2	1±0.1	1±0.1	1 ± 0.1	1 ± 0.5	1 ± 0.2	1 ± 0.3	1 ± 0.9
Asn909Lys	0.2 ± 0.03	0.4 ±0.1	0 ± 0	0 ± 0	0.01 ± 0.02	1.2 ± 0.7	0.9 ± 0.3	1.5 ± 1.3
His1221Arg	0.3 ± 0.08	0.2 ± 0.03	0.7 ± 0.2	1.2 ± 0.1	4.1 ± 1.7	4.2 ± 1.5	6.6 ± 3.9	3.8 ± 2.4
Ile703Val	0.4 ± 0.09	0.7 ± 0.07	0.9 ± 0.2	1.0 ± 0.2	1.1 ± 0.6	1.3 ± 0.3	1.9 ± 0.9	1.7 ± 1.0
Trp336Ala/Phe337Leu	0.5 ± 0.07	0.1 ± 0.04	0 ± 0	0 ± 0	0 ± 0	6.4 ± 3.1	3.3 ± 1.6	4.6 ± 3.2

XDH, to the more detrimental oxidized isoform, XO. Because of this modification, the XDH/XO ratio shifts in favour of oxygen radical production. Our study demonstrates, for the first time, that the SNPs leading to non-synonymous substitutions have a critical role in determining XDH/XO proportion. We observed that Ile703Val and His1221Arg exhibited a prevalence of the oxidase isoform of the enzyme over the dehydrogenase. It is possible that technical issues caused these differences. Previous studies suggest that sample processing conditions can cause conversion of the NAD^+-dependency to O_2-dependency [55] as also can low temperature storage [56]. Since all cells and samples were treated identically, these technical issues are unlikely to explain our observations. The His1221Arg mutant exhibited greater XO activity of 70% of the total compared to the WT (55%) and Ile703Val (57%); a difference we propose is likely not due to differences in post-translational modification but also likely a consequence of non-synonymous alteration of the peptide chain. Nishino et al. using a non-mammalian expression system, demonstrated that non-synonymous substitutions of key cysteine residues (Cys535Ala and Cys992Arg) prevent XDH oxidation [2].

Importantly, we acknowledge that of the mutations we tested only the artificial Trp336AlaPhe337Leu variant resides within the active site for $O_2^{\cdot-}$ production, however, our observations indicate that mutations distant from this site also impact biochemical activity. Interestingly, both Cys535 and 992 are well conserved across mammalian XDHs indicating the generalisability of this regulation across species. The one exception is chicken where the electrically neutral Cys992 is replaced by the positively charged Arg [57]. Furthermore, it is noteworthy that, whilst chicken Cys535 is followed by glutamic acid (Glu) at the position 536, mammalian Cys535 is followed by glycine (Gly). This difference, whilst seemingly unimportant, prevents the formation of a disulphide bridge leading to speculation that other adjacent amino acids may be critical in determining conversion [58]. This leads us to speculate that His1221 may still influence Cys(s) oxidation capacity and consequently XDH conversion to XO. Indeed, X-ray crystallography of purified bovine XOR showed that, when completely folded, regions considered spatially distant, i.e. the Mo–Pt domain and the interfaces of the Fe/S and FAD domains, come into close contact [59]. In keeping with these observations, our computational analysis reveals that His1221 interacts with the backbone and sidechain of Trp 1329 likely stabilising the loop structures in this region. Thus, the change to Arg may impact upon the oxidation process of adjacent amino acids, including Cys 1326 which has been also implicated in conversion of XDH to XO [2]. However, regardless of the nature of the process, reversible or irreversible, XDH conversion to XO is accompanied by a disruption of a central cluster (Arg 335, Trp 336, Arg 427, and Phe 550) with consequent conformational changes and relocation of the active loop A around the FAD site [2]. There is evidence that a double mutation Trp336Ala/Phe337Leu, also reproduced in our study, is accompanied by a loss of interaction of Phe 549 (human 550) favouring XO over the XDH structure [34].

Whilst most mutations identified in the *XDH* open reading frame have been associated with a reduced or abolished XOR activity [25], a few have been associated with an increased oxidase activity [23,60]. Of the 21 non-synonymous mutations previously identified, 10 exhibited significant differences in the kinetic parameters (Km, Vmax, Vmax/Km) of XOR-driven xanthine oxidation. Amongst these, only two, His1221Arg and Ile703Val, showed a significant increase in purinergic activity compared to the WT due to a substantial rise of Vmax [27], whereas Asn909Lys demonstrated a significant loss of activity. In agreement, we confirmed that the non-synonymous mutation of the *C*-terminal domain, His1221Arg, positively modulate the oxidase activity of the enzyme which may account for inter-individual variations of oxidative stress [23,24,60]. In addition to that, we also show for the first time a significant increase in $O_2^{\cdot-}$ production with His1221Arg in presence of different reducing agents, but, in contrast to Kudo *et al* [27], a similar activity for Ile703Val versus the WT. A plausible rationale for this discrepancy may be that in the Kudo et al. study, UA, a surrogate of XOR activity, was the only sub-product measured and the obtained values were not normalised to the enzyme expression levels. This explanation is further corroborated by our UA measurement which reveals important differences between pre- and post-normalization to XOR expression levels with His1221Arg causing statistically significant elevation of UA levels at baseline. The functional consequence of this is uncertain, and indeed much support for negative effects of excessive UA build-up exists within the literature. However, this view should be balanced with the knowledge that at baseline UA is thought to account for ~50% of the in vivo anti-oxidant capacity in humans [61,62].

Our findings regarding Asn909Lys activity also show differences to those previously reported [27,34]. Indeed, whilst Kudo et al. demonstrated a 4-fold reduction of Vmax compared to WT for UA synthesis highlighting the mutation as a potential cause of xanthinuria, our $O_2^{\cdot-}$ analysis only revealed a downward trend compared to hXDH WT, whereas UA quantification showed similar activity in presence of xanthine. In addition, when we exposed Asn909Lys to the FAD-reducing agent NADH and the activity was normalised to XOR expression, the Asn909Lys showed similar levels of $O_2^{\cdot-}$ to hXDH WT, suggesting that in Kudo et al. the reductions are likely due to lower levels of expression rather than lower activity per se. Similarly, the artificial double mutant, Trp335Ala/Phe336Leu (human Trp336Ala/Phe337Ala), suggested to be a highly $O_2^{\cdot-}$-producing enzyme [34], exhibited a profoundly reduced xanthine-driven dioxygen reduction capacity and no difference with NADH. However, when normalised to XOR expression level in the presence of NADH this mutant expressed a far greater production of $O_2^{\cdot-}$ than WT or His1221Arg; again, suggesting that the much lower expression level of the enzyme influenced perceived changes in activity should be considered.

It has been suggested that His1221Arg is localized at the surface of the Mo–Pt binding domain and, even though not directly involved in the formation of the active site cavity (Glu 803, Arg 881, Glu 1262), it positively modulates UA production by increasing its release rate [20]. There is also some evidence suggesting that chemical modification of surface amino acid residues slow XOR activity with a consequent reduction in urate release [63]. Taken together, these observations confirm the direct involvement of previously thought non-critical amino acid residues in the oxidation process of purines to UA, offering a plausible explanation for the increased $O_2^{\cdot-}$ production observed with His1221Arg in this study. We suggest that the increase in dioxygen reduction observed in this study, results from a combination of increased oxidase activity, coupled with altered XDH/XO proportion. These observations highlight the potential that His1221Arg expression may be a potential marker of hyperuricemia, oxidative stress, and endothelial

dysfunction.

The functional remit of XOR has extended well beyond ROS and UA synthesis over the past 10–15 years, with the growing appreciation that in many pathological settings, particularly for metabolic disease and CVD, when the eNOS-dependent pathway is dysfunctional, XOR acts as a critical NO_2^--reductase [9], [64–66]. Thus, the increase in NO_2^- reduction to ·NO observed in this study with some of the naturally occurring mutations may be particularly important for health. NO_2^--reductase activity for His1221Arg and Trp336Ala/Phe337Leu was elevated in comparison to WT with a trend for Ile703Val. This finding opens a new important question about the potential protective role of Ile703Val and His1221Arg which warrants further structural and molecular investigations.

To interrogate more closely the possibility that non-synonymous mutations may alter the enzymatic tertiary structure and consequently the intramolecular shuttling of electrons, we investigated the NO_2^--reductase activity in the presence of NADH, or xanthine. These substrates did not influence ·NO generation from NO_2^- in HEK-293, Asn909Lys or Trp336Ala/Phe337Leu cell lysate. In contrast for cells expressing hXDH WT, His1221Arg or Ile703Val, NO_2^- reduction was facilitated in the presence of both reducing agents, with His1221Arg showing a preference for xanthine over NADH. Taken together these findings suggest that in His1221Arg, the two redox centres Fe/S I and II are still functional and efficiently shuttling electrons between the Mo–Pt and FAD sites; both xanthine- and NADH-derived electrons are able to catalyse dioxygen and NO_2^- reductions; and finally, the electrons passed to the enzyme are preferentially used at the same site of production and thus His1221Arg showing a tendency of more efficiently using xanthine over NADH and vice versa for Ile703Val. These observations, albeit exploratory, suggest that non-synonymous mutations of the enzyme may change its affinity for Mo–Pt or FAD specific substrate. Considering that purines and NADH concentrations change dramatically before and after a pathological insult, such as ischemia, this aspect warrants further investigations.

We acknowledge that our study utilises an in vitro expression system and thus whilst the cell system is of human origin further in vitro and in vivo analysis of the consequences of these mutations is needed. This can be addressed by purification of proteins and creation of transgenic mouse models as well as greater scrutiny of large genome-wide-association-study (GWAS) for further confirmation through replication. Since many known mutations of XDH are rare, recent advances in testing the impact of rare mutations upon key disease traits and markers is warranted.

5. Conclusion

This study has shown for the first time that a naturally occurring non-synonymous mutation of human XDH, His1221Arg leads to an altered XDH/XO proportion and an increased oxidase activity; effects typically seen in numerous pathological conditions. However, we have also demonstrated for the first time that the upregulation of XOR activity is accompanied by a substantial rise in its NO_2^--reductase potential. Moreover, in the presence of inorganic NO_2^-, these variants lead to increased generation of bioavailable NO coupled with a concomitant reduction of ROS and potentially UA. We also suggest that specific mutations such as Ile703Val, with a similar oxidase activity of WT but potentially increased NO_2^--reductase activity, may exert a biologically important effect in preventing aspects of CVD (Table 2). Collectively, these data lead us to speculate that carriers of a potential detrimental mutation, His1221Arg, may revert their latent pathological phenotype to a more beneficial one by targeting the non-canonical pathway for ·NO generation through the safe application of dietary inorganic nitrate (NO_3^-). With emerging evidence suggesting elevated sUA, ROS, and ·NO depletion as key markers of CVD, identification of pro-oxidative and uricaemic genotypes would allow potential stratification to treatments that might be useful in elevating NO levels leading to health benefits.

This article contains supplementary materials.

Funding

GM was partially supported by Menarini Ricerche, Italy (awarded to Prof Claudio Borghi) and the Italian society of Pharmacology (SIF). This work and GM were also supported by The Barts Charity Cardiovascular Programme (MRG00913). Nicki Dyson is funded by a BHF MRes/PhD Studentship (FS/19/62/34901).

Declaration of competing interest

The authors declare the following financial interests/personal relationships which may be considered as potential competing interests: Amrita Ahluwalia is a Co-Director of a small start-up Heartbeet Ltd seeking to identify therapeutic opportunities for dietary nitrate.

Data availability

Data will be made available on request.

Acknowledgments

General: We would like to express our gratitude to Professor Richard M. Wright for providing the pcDNA.3.1-myc-hysA-hXDH plasmid vector.

Appendix A. Supplementary data

Supplementary data to this article can be found online at https://doi.org/10.1016/j.redox.2023.102864.

References

[1] E.D. Corte, F. Stirpe, The regulation of rat liver xanthine oxidase. Involvement of thiol groups in the conversion of the enzyme activity from dehydrogenase (type D) into oxidase (type O) and purification of the enzyme, Biochem. J. 126 (1972) 739–745.
[2] T. Nishino, K. Okamoto, Y. Kawaguchi, H. Hori, T. Matsumura, B.T. Eger, E.F. Pai, Mechanism of the conversion of xanthine dehydrogenase to xanthine oxidase: identification of the two cysteine disulfide bonds and crystal structure of a non-convertible rat liver xanthine dehydrogenase mutant, J. Biol. Chem. 280 (2005) 24888–24894.
[3] M. Dixon, S. Thurlow, Studies on xanthine oxidase: the dynamics of the oxidase system, Biochem. J. 18 (1924) 976–988.
[4] R. Hille, T. Nishino, Flavoprotein structure and mechanism. 4. Xanthine oxidase and xanthine dehydrogenase, Faseb. J. 9 (1995) 995–1003.
[5] S.A. Sanders, R. Eisenthal, R. Harrison, NADH oxidase activity of human xanthine oxidoreductase–generation of superoxide anion, Eur. J. Biochem. 245 (1997) 541–548.
[6] Z. Zhang, D. Naughton, P.G. Winyard, N. Benjamin, D.R. Blake, M.C. Symons, Generation of nitric oxide by a nitrite reductase activity of xanthine oxidase: a potential pathway for nitric oxide formation in the absence of nitric oxide synthase activity, Biochem. Biophys. Res. Commun. 249 (1998) 767–772.
[7] C.M. Harris, V. Massey, The reaction of reduced xanthine dehydrogenase with molecular oxygen. Reaction kinetics and measurement of superoxide radical, J. Biol. Chem. 272 (1997) 8370–8379.
[8] T.M. Millar, C.R. Stevens, N. Benjamin, R. Eisenthal, R. Harrison, D.R. Blake, Xanthine oxidoreductase catalyses the reduction of nitrates and nitrite to nitric oxide under hypoxic conditions, FEBS Lett. 427 (1998) 225–228.
[9] V. Kapil, R.S. Khambata, D.A. Jones, K. Rathod, C. Primus, G. Massimo, J. M. Fukuto, A. Ahluwalia, The noncanonical pathway for in vivo nitric oxide generation: the nitrate-nitrite-nitric oxide pathway, Pharmacol. Rev. 72 (2020) 692–766.
[10] N. Dalbeth, A.L. Gosling, A. Gaffo, A. Abhishek, Gout, Lancet 397 (2021) 1843–1855.
[11] M. Kuwabara, C. Borghi, A.F.G. Cicero, I. Hisatome, K. Niwa, M. Ohno, R. J. Johnson, M.A. Lanaspa, Elevated serum uric acid increases risks for developing high LDL cholesterol and hypertriglyceridemia: a five-year cohort study in Japan, Int. J. Cardiol. 261 (2018) 183–188.
[12] C.E. Berry, J.M. Hare, Xanthine oxidoreductase and cardiovascular disease: molecular mechanisms and pathophysiological implications, J. Physiol. 555 (2004) 589–606.
[13] D.I. Feig, M. Madero, D.I. Jalal, L.G. Sanchez-Lozada, R.J. Johnson, Uric acid and the origins of hypertension, J. Pediatr. 162 (2013) 896–902.

[14] A.F.G. Cicero, P. Salvi, S. D'Addato, M. Rosticci, C. Borghi, g for the Brisighella Heart Study, Association between serum uric acid, hypertension, vascular stiffness and subclinical atherosclerosis: data from the Brisighella Heart Study, J. Hypertens. 32 (2014).

[15] R.S. Khambata, S.M. Ghosh, A. Ahluwalia, "Repurposing" of xanthine oxidoreductase as a nitrite reductase: a new paradigm for therapeutic targeting in hypertension, Antioxidants Redox Signal. 23 (2015) 340–353.

[16] P. Tripatara, N.S. Patel, A. Webb, K. Rathod, F.M. Lecomte, E. Mazzon, S. Cuzzocrea, M.M. Yaqoob, A. Ahluwalia, C. Thiemermann, Nitrite-derived nitric oxide protects the rat kidney against ischemia/reperfusion injury in vivo: role for xanthine oxidoreductase, J. Am. Soc. Nephrol. 18 (2007) 570–580.

[17] S. Velmurugan, J.M. Gan, K.S. Rathod, R.S. Khambata, S.M. Ghosh, A. Hartley, S. Van Eijl, V. Sagi-Kiss, T.A. Chowdhury, M. Curtis, G.G. Kuhnle, W.G. Wade, A. Ahluwalia, Dietary nitrate improves vascular function in patients with hypercholesterolemia: a randomized, double-blind, placebo-controlled study, Am. J. Clin. Nutr. 103 (2016) 25–38.

[18] M. Peleli, C. Zollbrecht, M.F. Montenegro, M. Hezel, J. Zhong, E.G. Persson, R. Holmdahl, E. Weitzberg, J.O. Lundberg, M. Carlstrom, Enhanced XOR activity in eNOS-deficient mice: effects on the nitrate-nitrite-NO pathway and ROS homeostasis, Free Radic. Biol. Med. 99 (2016) 472–484.

[19] N. Arikyants, A. Sarkissian, A. Hesse, T. Eggermann, E. Leumann, B. Steinmann, Xanthinuria type I: a rare cause of urolithiasis, Pediatr. Nephrol. 22 (2007) 310–314.

[20] K. Ichida, Y. Amaya, K. Okamoto, T. Nishino, Mutations associated with functional disorder of xanthine oxidoreductase and hereditary xanthinuria in humans, Int. J. Mol. Sci. 13 (2012) 15475–15495.

[21] A. Tin, O.M. Woodward, W.H. Kao, C.T. Liu, X. Lu, M.A. Nalls, D. Shriner, M. Semmo, E.L. Akylbekova, S.B. Wyatt, S.J. Hwang, Q. Yang, A.B. Zonderman, A. A. Adeyemo, C. Palmer, Y. Meng, M. Reilly, M.G. Shlipak, D. Siscovick, M.K. Evans, C.N. Rotimi, M.F. Flessner, M. Kottgen, L.A. Cupples, C.S. Fox, A. Kottgen, Care, C. Consortia, Genome-wide association study for serum urate concentrations and gout among African Americans identifies genomic risk loci and a novel URAT1 loss-of-function allele, Hum. Mol. Genet. 20 (2011) 4056–4068.

[22] L.E.J.M. Scheepers, F.-F. Wei, K. Stolarz-Skrzypek, S. Malyutina, V. Tikhonoff, L. Thijs, E. Salvi, C. Barlassina, J. Filipovský, E. Casiglia, Y. Nikitin, K. Kawecka-Jaszcz, P. Manunta, D. Cusi, A. Boonen, J.A. Staessen, I.C.W. Arts, Xanthine oxidase gene variants and their association with blood pressure and incident hypertension: a population study, J. Hypertens. 34 (2016).

[23] J. Yang, K. Kamide, Y. Kokubo, S. Takiuchi, T. Horio, T. Matayoshi, H. Yasuda, Y. Miwa, M. Yoshii, F. Yoshihara, S. Nakamura, H. Nakahama, H. Tomoike, T. Miyata, Y. Kawano, Associations of hypertension and its complications with variations in the xanthine dehydrogenase gene, Hypertens. Res. 31 (2008) 931–940.

[24] F.J. Chaves, D. Corella, S. Blesa, M.L. Mansego, P. Marin, O. Portoles, J.V. Sorli, V. Gonzalez-Albert, M.C. Tormos, A.B. Garcia-Garcia, G. Saez, J. Redon, Xanthine oxidoreductase polymorphisms: influence in blood pressure and oxidative stress levels, Pharmacogenetics Genom. 17 (2007) 589–596.

[25] N. Sakamoto, T. Yamamoto, Y. Moriwaki, T. Teranishi, M. Toyoda, Y. Onishi, S. Kuroda, K. Sakaguchi, T. Fujisawa, M. Maeda, T. Hada, Identification of a new point mutation in the human xanthine dehydrogenase gene responsible for a case of classical type I xanthinuria, Hum. Genet. 108 (2001) 279–283.

[26] Y. Kuwabara, T. Nishino, K. Okamoto, T. Matsumura, B.T. Eger, E.F. Pai, T. Nishino, Unique amino acids cluster for switching from the dehydrogenase to oxidase form of xanthine oxidoreductase, Proc. Natl. Acad. Sci. U. S. A. 100 (2003) 8170–8175.

[27] M. Kudo, T. Moteki, T. Sasaki, Y. Konno, S. Ujiie, A. Onose, M. Mizugaki, M. Ishikawa, M. Hiratsuka, Functional characterization of human xanthine oxidase allelic variants, Pharmacogenetics Genom. 18 (2008) 243–251.

[28] A. Iguchi, T. Sato, M. Yamazaki, K. Tasaki, Y. Suzuki, N. Iino, H. Hasegawa, K. Ichida, I. Narita, A case of xanthinuria type I with a novel mutation in xanthine dehydrogenase, CEN Case Rep. 5 (2016) 158–162.

[29] Zhang, D., Yang, M., Zhou, D., Li, Z., Cai, L., Bao, Y., Li, H., Shan, Z., Liu, J., Lv, D., Liu, Y., Xu, C., Ling, J., Xu, Y., Zhang, S., Huang, Q., Shi, Y., Zhu, Y., and Lai, M. The Polymorphism Rs671 at ALDH2 Associated with Serum Uric Acid Levels in Chinese Han Males: A Genome-wide Association Study..

[30] L. Zhang, K.L. Spencer, V.S. Voruganti, N.W. Jorgensen, M. Fornage, L.G. Best, K. D. Brown-Gentry, S.A. Cole, D.C. Crawford, E. Deelman, N. Franceschini, A. L. Gaffo, K.R. Glenn, G. Heiss, N.S. Jenny, A. Kottgen, Q. Li, K. Liu, T.C. Matise, K. E. North, J.G. Umans, W.H.L. Kao, Association of functional polymorphism rs2231142 (Q141K) in the ABCG2 gene with serum uric acid and gout in 4 US populations: the PAGE study, Am. J. Epidemiol. 177 (2013) 923–932.

[31] M.J. Caulfield, P.B. Munroe, D. O'Neill, K. Witkowska, F.J. Charchar, M. Doblado, S. Evans, S. Eyheramendy, A. Onipinla, P. Howard, S. Shaw-Hawkins, R.J. Dobson, C. Wallace, S.J. Newhouse, M. Brown, J.M. Connell, A. Dominiczak, M. Farrall, G. M. Lathrop, N.J. Samani, M. Kumari, M. Marmot, E. Brunner, J. Chambers, P. Elliott, J. Kooner, M. Laan, E. Org, G. Veldre, M. Viigimaa, F.P. Cappuccio, C. Ji, R. Iacone, P. Strazzullo, K.H. Moley, C. Cheeseman, SLC2A9 is a high-capacity urate transporter in humans, PLoS Med. 5 (2008) e197.

[32] A. Tin, J. Marten, V.L.H. Kuhns, Y. Li, M. Wuttke, H. Kirsten, K.B. Sieber, C.X. Qiu, M. Gorski, Z. Yu, A. Giri, G. Sveinbjornsson, M. Li, A.Y. Chu, A. Hoppmann, L. J. O'Connor, B. Prins, T. Nutile, D. Noce, M. Akiyama, M. Cocca, S. Ghasemi, P. J. van Der Most, K. Horn, Y.Z. Xu, C. Fuchsberger, S. Sedaghat, S. Afaq, N. Amin, J. Arnlo, S.J.L. Bakker, N. Bansal, D. Baptista, S. Bergmann, M.L. Biggs, G. Biino, E. Boerwinkle, E.P. Bottinger, T.S. Boutin, M. Brumat, R. Burkhardt, E. Campana, A. Campbell, H. Campbell, R.J. Carroll, E. Catamo, J.C. Chambers, M. Ciullo, M. P. Concas, J. Coresh, T. Corre, D. Cusi, S.C. Felicita, M.H. de Borst, A. De Grandi, R. de Mutsert, A.P.J. de Vries, G. Delgado, A. Demirkan, O. Devuyst, K. Dittrich, K. U. Eckardt, G. Ehret, K. Endlich, M.K. Evans, R.T. Gansevoort, P. Gasparini, V. Giedraitis, C. Gieger, G. Girotto, M. Ggele, S.D. Gordon, D.F. Gudbjartsson, V. Gudnason, T. Haller, P. Hamet, T.B. Harris, C. Hayward, A.A. Hicks, E. Hofer, H. Holm, W. Huang, N. Hutri-Kahonen, S.J. Hwang, M.A. Ikram, R.M. Lewis, E. Ingelsson, J. Jakobsdottir, I. Jonsdottir, H. Jonsson, P.K. Joshi, N.S. Josyula, B. Jung, M. Kahonen, Y. Kamatani, M. Kanai, S.M. Kerr, W. Kiess, M.E. Kleber, W. Koenig, J.S. Kooner, A. Korner, P. Kovacs, B.K. Kramer, F. Kronenberg, M. Kubo, B. Kuhnel, M. La Bianca, L.A. Lange, B. Lehne, T. Lehtimaki, J. Liu, M. Loeffler, R.J. F. Loos, L.P. Lyytikainen, R. Magi, A. Mahajan, N.G. Martin, W. Marz, D. Mascalzoni, K. Matsuda, C. Meisinger, T. Meitinger, A. Metspalu, Y. Milaneschi, C.J. Odonnell, O.D. Wilson, J.M. Gaziano, P.P. Mishra, K.L. Mohlke, N. Mononen, G.W. Montgomery, D.O. Mook-Kanamori, M. Muller-Nurasyid, G.N. Nadkarni, M. A. Nalls, M. Nauck, K. Nikus, B.T. Ning, I.M. Nolte, R. Noordam, J.R. O'Connell, I. Olafsson, S. Padmanabhan, B.W.J.H. Penninx, T. Perls, A. Peters, M. Pirastu, N. Pirastu, G. Pistis, O. Polasek, B. Ponte, D.J. Porteous, T. Poulain, M.H. Preuss, T. J. Rabelink, L.M. Raffield, O.T. Raitakari, R. Rettig, M. Rheinberger, K.M. Rice, F. Rizzi, A. Robino, I. Rudan, A. Krajcoviechova, R. Cifkova, R. Rueedi, D. Ruggiero, K.A. Ryan, Y. Saba, E. Salvi, H. Schmidt, R. Schmidt, C.M. Shaffer, A. V. Smith, B.H. Smith, C.N. Spracklen, K. Strauch, M. Stumvoll, P. Sulem, S. M. Tajuddin, A. Teren, J. Thiery, C.H.L. Thio, U. Thorsteinsdottir, D. Toniolo, A. Tonjes, J. Tremblay, A.G. Uitterlinden, S. Vaccargiu, P. van der Harst, C.M. van Duijn, N. Verweij, U. Volker, P. Vollenweider, G. Waeber, M. Waldenberger, J. B. Whitfield, S.H. Wild, J.F. Wilson, Q. Yang, W.H. Zhang, A.B. Zonderman, M. Bochud, J.G. Wilson, S.A. Pendergrass, K. Ho, A. Parsa, P.P. Pramstaller, B. M. Psaty, C.A. Boger, H. Snieder, A.S. Butterworth, Y. Okada, T.L. Edwards, K. Stefansson, K. Susztak, M. Scholz, I.M. Heid, A.M. Hung, A. Teumer, C. Pattaro, O.M. Woodward, V. Vitart, A. Kottgen, G.C.K.D. Study, L.C. Study, V.M. V. Program, Target genes, variants, tissues and transcriptional pathways influencing human serum urate levels, Nat. Genet. 51 (2019), 1459-+.

[33] M. Kudo, T. Sasaki, M. Ishikawa, N. Hirasawa, M. Hiratsuka, Functional characterization of genetic polymorphisms identified in the promoter region of the xanthine oxidase gene, Drug Metabol. Pharmacokinet. 25 (2010) 599–604.

[34] R. Asai, T. Nishino, T. Matsumura, K. Okamoto, K. Igarashi, E.F. Pai, Two mutations convert mammalian xanthine oxidoreductase to highly superoxide-productive xanthine oxidase, J. Biochem. 141 (2007) 525–534.

[35] S. Haglund, S. Vikingsson, S. Almer, J. Soderman, Combination treatment with 6-mercaptopurine and allopurinol in HepG2 and HEK293 cells - effects on gene expression levels and thiopurine metabolism, PLoS One 12 (2017), e0173825.

[36] J.S. Beckman, D.A. Parks, J.D. Pearson, P.A. Marshall, B.A. Freeman, A sensitive fluorometric assay for measuring xanthine dehydrogenase and oxidase in tissues, Free Radic. Biol. Med. 6 (1989) 607–615.

[37] T. Munzel, I.B. Afanas'ev, A.L. Kleschyov, D.G. Harrison, Detection of superoxide in vascular tissue, Arterioscler. Thromb. Vasc. Biol. 22 (2002) 1761–1768.

[38] S.M. Ghosh, V. Kapil, I. Fuentes-Calvo, K.J. Bubb, V. Pearl, A.B. Milsom, R. Khambata, S. Maleki-Toyserkani, M. Yousuf, N. Benjamin, A.J. Webb, M. J. Caulfield, A.J. Hobbs, A. Ahluwalia, Enhanced vasodilator activity of nitrite in hypertension: critical role for erythrocytic xanthine oxidoreductase and translational potential, Hypertension 61 (2013) 1091–1102.

[39] J.S. McNally, M.E. Davis, D.P. Giddens, A. Saha, J. Hwang, S. Dikalov, H. Jo, D. G. Harrison, Role of xanthine oxidoreductase and NAD(P)H oxidase in endothelial superoxide production in response to oscillatory shear stress, Am. J. Physiol. Heart Circ. Physiol. 285 (2003) H2290–H2297.

[40] J.S. McNally, A. Saxena, H. Cai, S. Dikalov, D.G. Harrison, Regulation of xanthine oxidoreductase protein expression by hydrogen peroxide and calcium, Arterioscler. Thromb. Vasc. Biol. 25 (2005) 1623–1628.

[41] H. Li, A. Samouilov, X. Liu, J.L. Zweier, Characterization of the magnitude and kinetics of xanthine oxidase-catalyzed nitrite reduction. Evaluation of its role in nitric oxide generation in anoxic tissues, J. Biol. Chem. 276 (2001) 24482–24489.

[42] K. Ichida, Y. Amaya, K. Okamoto, T. Nishino, Mutations associated with functional disorder of xanthine oxidoreductase and hereditary xanthinuria in humans, Int. J. Mol. Sci. 13 (2012) 15475–15495.

[43] M. Kudo, T. Moteki, T. Sasaki, Y. Konno, S. Ujiie, A. Onose, M. Mizugaki, M. Ishikawa, M. Hiratsuka, Functional characterization of human xanthine oxidase allelic variants, Pharmacogenetics Genom. 18 (2008) 243–251.

[44] S. Angermuller, G. Bruder, A. Volkl, H. Wesch, H.D. Fahimi, Localization of xanthine oxidase in crystalline cores of peroxisomes. A cytochemical and biochemical study, Eur. J. Cell Biol. 45 (1987) 137–144.

[45] M. Rouquette, S. Page, R. Bryant, M. Benboubetra, C.R. Stevens, D.R. Blake, W. D. Whish, R. Harrison, D. Tosh, Xanthine oxidoreductase is asymmetrically localised on the outer surface of human endothelial and epithelial cells in culture, FEBS (Fed. Eur. Biochem. Soc.) Lett. 426 (1998) 397–401.

[46] A. Narula, J. Ellis, J.M. Taliaferro, O.S. Rissland, Coding regions affect mRNA stability in human cells, RNA 25 (2019) 1751–1764.

[47] K.D. Pfeffer, T.P. Hueckstedt, J.R. Hoidal, Xanthine dehydrogenase and xanthine oxidase activity and gene expression in renal epithelial cells. Cytokine and steroid regulation, J. Immunol. 153 (1994) 1789–1797.

[48] G.P. Dupont, T.P. Hueckstedt, B.C. Marshall, U.S. Ryan, J.R. Michael, J.R. Hoidal, Regulation of xanthine dehydrogenase and xanthine oxidase activity and gene expression in cultured rat pulmonary endothelial cells, J. Clin. Invest. 89 (1992) 197–202.

[49] S. Page, D. Powell, M. Benboubetra, C.R. Stevens, D.R. Blake, F. Selase, A. J. Wolstenholme, R. Harrison, Xanthine oxidoreductase in human mammary epithelial cells: activation in response to inflammatory cytokines, Biochim. Biophys. Acta 1381 (1998) 191–202.

[50] C. Xu, X. Wan, L. Xu, H. Weng, M. Yan, M. Miao, Y. Sun, G. Xu, S. Dooley, Y. Li, C. Yu, Xanthine oxidase in non-alcoholic fatty liver disease and hyperuricemia: one stone hits two birds, J. Hepatol. 62 (2015) 1412–1419.
[51] J. Fallica, L. Varela, L. Johnston, B. Kim, L. Serebreni, L. Wang, M. Damarla, T. M. Kolb, P.M. Hassoun, R. Damico, Macrophage migration inhibitory factor: a novel inhibitor of apoptosis signal-regulating kinase 1-p38-Xanthine oxidoreductase-dependent cigarette smoke-induced apoptosis, Am. J. Respir. Cell Mol. Biol. 54 (2016) 504–514.
[52] L.S. Terada, D. Piermattei, G.N. Shibao, J.L. McManaman, R.M. Wright, Hypoxia regulates xanthine dehydrogenase activity at pre- and posttranslational levels, Arch. Biochem. Biophys. 348 (1997) 163–168.
[53] L.S. Terada, D.M. Guidot, J.A. Leff, I.R. Willingham, M.E. Hanley, D. Piermattei, J. E. Repine, Hypoxia injures endothelial cells by increasing endogenous xanthine oxidase activity, Proc. Natl. Acad. Sci. U. S. A. 89 (1992) 3362–3366.
[54] S.M. Ghosh, V. Kapil, I. Fuentes-Calvo, K.J. Bubb, V. Pearl, A.B. Milsom, R. Khambata, S. Maleki-Toyserkani, M. Yousuf, N. Benjamin, A.J. Webb, M. J. Caulfield, A.J. Hobbs, A. Ahluwalia, Enhanced vasodilator activity of nitrite in hypertension: critical role for erythrocytic xanthine oxidoreductase and translational potential, Hypertension 61 (2013) 1091–1102.
[55] F. Stirpe, E. Della Corte, The regulation of rat liver xanthine oxidase. Conversion in vitro of the enzyme activity from dehydrogenase (type D) to oxidase (type O), J. Biol. Chem. 244 (1969) 3855–3863.
[56] D.G. Blair, B.D. McLennan, Intensification of the xanthine oxidase activity of rat liver homogenates on storage, Can. J. Biochem. 46 (1968) 1047–1056.
[57] A. Sato, T. Nishino, K. Noda, Y. Amaya, The structure of chicken liver xanthine dehydrogenase. cDNA cloning and the domain structure, J. Biol. Chem. 270 (1995) 2818–2826.
[58] T. Nishino, The conversion from the dehydrogenase type to the oxidase type of rat liver xanthine dehydrogenase by modification of cysteine residues with fluorodinitrobenzene, J. Biol. Chem. 272 (1997) 29859–29864.
[59] C. Enroth, B.T. Eger, K. Okamoto, T. Nishino, E.F. Pai, Crystal structures of bovine milk xanthine dehydrogenase and xanthine oxidase: structure-based mechanism of conversion, Proc. Natl. Acad. Sci. U. S. A. 97 (2000) 10723–10728.
[60] L.E. Scheepers, F.F. Wei, K. Stolarz-Skrzypek, S. Malyutina, V. Tikhonoff, L. Thijs, E. Salvi, C. Barlassina, J. Filipovský, E. Casiglia, Y. Nikitin, K. Kawecka-Jaszcz, P. Manunta, D. Cusi, A. Boonen, J.A. Staessen, I.C. Arts, Xanthine oxidase gene variants and their association with blood pressure and incident hypertension: a population study, J. Hypertens. 34 (2016) 2147–2154.
[61] B.N. Ames, R. Cathcart, E. Schwiers, P. Hochstein, Uric acid provides an antioxidant defense in humans against oxidant- and radical-caused aging and cancer: a hypothesis, Proc. Natl. Acad. Sci. U. S. A. 78 (1981) 6858–6862.
[62] Y.Y. Sautin, R.J. Johnson, Uric acid: the oxidant-antioxidant paradox, Nucleos Nucleot. Nucleic Acids 27 (2008) 608–619.
[63] T. Nishino, K. Tsushima, R. Hille, V. Massey, Inhibition of milk xanthine oxidase by fluorodinitrobenzene, J. Biol. Chem. 257 (1982) 7348–7353.
[64] L.C. Gee, G. Massimo, C. Lau, C. Primus, D. Fernandes, J. Chen, K.S. Rathod, A.J. P. Hamers, F. Filomena, G. Nuredini, A.S. Ibrahim, R.S. Khambata, A.K. Gupta, J. C. Moon, V. Kapil, A. Ahluwalia, Inorganic nitrate attenuates cardiac dysfunction: roles for xanthine oxidoreductase and nitric oxide, Br. J. Pharmacol. 179 (2022) 4757–4777.
[65] R.S. Khambata, S.M. Ghosh, K.S. Rathod, T. Thevathasan, F. Filomena, Q. Xiao, A. Ahluwalia, Antiinflammatory actions of inorganic nitrate stabilize the atherosclerotic plaque, Proc. Natl. Acad. Sci. U. S. A. 114 (2017) E550–E559.
[66] M. Hezel, M. Peleli, M. Liu, C. Zollbrecht, B.L. Jensen, A. Checa, A. Giulietti, C. E. Wheelock, J.O. Lundberg, E. Weitzberg, M. Carlström, Dietary nitrate improves age-related hypertension and metabolic abnormalities in rats via modulation of angiotensin II receptor signaling and inhibition of superoxide generation, Free Radic. Biol. Med. 99 (2016) 87–98.

Abbreviations

AUC: Area Under the Curve
Asn909Lys: Asparagine909Lysine
CVD: Cardiovascular disease
CPS: Count per second
Cys: Cysteine
DPI: Diphenyleneiodonium
FAD: Flavin adenine dinucleotide
GWAS: Genome-wide-association study
His1221Arg: Histidine1221Arginin
HEK-293: Human Embryonic Kidney
hXDH WT: Human Xanthine Dehydrogenase wild-type
H_2O_2*:* Hydrogen peroxide
Fe–S: Iron-sulphur
Ile703Val: Isoleucine703Valine
LECL: Lucigenin-enhanced chemiluminescence
MHRA: Medicines and Healthcare products Regulatory Agency
Mo–Pt: Molybdo-Pterine
NAD^+*:* Nicotinamide adenine dinucleotide
NADH: Nicotinamide adenine dinucleotide hydrogen
NO_3^-*:* Nitrate
NO_2^-*:* Nitrite
NO: Nitric oxide
O_2*:* Oxygen
ROS: Reactive oxygen species
Trp336Ala/Phe337Leu or Trp336Ala: Tryptophan336Alanine/Phenylalanine337Leucine
SNPs: Single nucleotide polymorphisms
$O_2^{\cdot-}$*:* Superoxide anion
UA: Uric acid
XDH: Xanthine dehydrogenase
XOR: Xanthine Oxidoreductase
XO: Xanthine Oxidase